Contrasting sensitivity of lake sediment *n*-alkanoic acids and *n*-alkanes to basin-scale vegetation and regional-scale precipitation δ^2H in the Adirondack Mountains, NY (USA)

Erika J. Freimuth[a,*], Aaron F. Diefendorf[a], Thomas V. Lowell[a], Benjamin R. Bates[a], Anna Schartman[a], Broxton W. Bird[b], Joshua D. Landis[c], Alexander K. Stewart[d]

[a] Department of Geology, University of Cincinnati, Cincinnati, OH 45221-0013, USA

[b] Department of Earth Sciences, Indiana University-Purdue University, Indianapolis, IN 46202, USA

[c] Department of Earth Sciences, Dartmouth College, Hanover, NH 03755-3571, USA

[d] Department of Geology, St. Lawrence University, Canton, NY 13617, USA

[*]Corresponding author. Tel. : +1-631-553-3918.

E-mail address: erika.freimuth@gmail.com (E.J. Freimuth).

Keywords: Hydrogen isotopes; plant wax; aquatic biomarkers; lacustrine sediment

---

This is the author's manuscript of the article published in final edited form as:

Freimuth, E. J., Diefendorf, A. F., Lowell, T. V., Bates, B. R., Schartman, A., Bird, B. W., … Stewart, A. K. (2019). Contrasting sensitivity of lake sediment n-alkanoic acids and n-alkanes to basin-scale vegetation and regional-scale precipitation δ2H in the Adirondack Mountains, NY (USA). Geochimica et Cosmochimica Acta, 268, pp. 22-41. https://doi.org/10.1016/j.gca.2019.08.026

ABSTRACT

The hydrogen isotope values of plant waxes (δ^2H_{wax}) primarily reflect plant source water. δ^2H_{wax} preserved in lake sediments has therefore been widely used to investigate past hydroclimate. The processes by which plant waxes are integrated at regional and catchment scales are poorly understood and may affect the δ^2H_{wax} values recorded in sediments. Here, we assess the variability of sedimentary δ^2H_{wax} for two plant wax compound classes (*n*-alkanes and *n*-alkanoic acids) across 12 lakes in the Adirondack Mountains that receive similar regional precipitation δ^2H but vary at the catchment-scale in terms of vegetation structure and basin morphology. Total long-chain (*n*-C_{27} to *n*-C_{35}) alkane concentrations were similar across all sites (191 ± 53 µg/g TOC) while total long-chain (*n*-C_{28} and *n*-C_{30}) alkanoic acid concentrations were more variable (117 ± 116 µg/g TOC) and may reflect shoreline vegetation composition. Lakes with shorelines dominated by evergreen gymnosperm plants had significantly higher concentrations of long-chain *n*-alkanoic acids relative to *n*-alkanes, consistent with our observations that deciduous angiosperms produced more long-chain *n*-alkanes than evergreen gymnosperms (471 and 33 µg/g TOC, respectively). In sediments, the most abundant chain lengths in each compound class were *n*-C_{29} alkane and *n*-C_{28} alkanoic acid, which had mean δ^2H values of -188 ± 6‰ and -164 ± 9‰, respectively. Across sites, the range in sedimentary *n*-C_{29} alkane (22‰) and *n*-C_{28} alkanoic acid δ^2H (35‰) was larger than expected based on the total range in modeled mean annual precipitation δ^2H (4‰). We observed larger mean ε_{app} (based on absolute values) for *n*-alkanes (-123‰) than for *n*-alkanoic acids (-97‰). Across sites, the δ^2H offset between *n*-C_{29} alkane and the biosynthetic precursor *n*-C_{30} alkanoic acid ($\varepsilon_{C29\text{-}C30}$) ranged from -8 to -58‰, which was more variable than expected based on observations in temperate trees (-20 to -30‰). Sediments with greater aquatic organic matter contributions (lower C/N ratios) had significantly larger (absolute) $\varepsilon_{C29\text{-}C30}$ values, which may reflect long-chain *n*-alkanoic acids from aquatic sources. Concentration and δ^2H_{wax} data in Adirondack lakes suggest that long-chain *n*-alkanes are more sensitive to regional-scale precipitation signals, while *n*-alkanoic acids are more

sensitive to basin-scale differences in catchment vegetation and wax sourcing.

1. Introduction

The hydrogen isotopic composition of plant waxes (δ^2H_{wax}) has become an important tool for reconstructing paleohydrology (Pancost and Boot, 2004; Castañeda and Schouten, 2011; Sachse et al., 2012; Sessions, 2016). Plants synthesize leaf waxes using hydrogen derived from plant source waters (including soil, stream and lake water), which are derived from precipitation. δ^2H_{wax} is therefore interpreted to reflect the δ^2H composition of precipitation (δ^2H_p) from which the plant's water was ultimately sourced (Sachse et al., 2006; Feakins and Sessions, 2010; Kahmen et al., 2013a; Kahmen et al., 2013b; Tipple and Pagani, 2013). The relationship between δ^2H_p and δ^2H_{wax} persists from the plant-level to both marine and lacustrine sediments, which can serve as tools for reconstructing plant source water (i.e., precipitation) throughout the Cenozoic (e.g., Tierney et al., 2008; Niedermeyer et al., 2014; Carmichael et al., 2017).

Molecular paleohydrology relies upon estimates of the net apparent fractionation (ε_{app}) between δ^2H_p and δ^2H_{wax}. While ε_{app} is critical for calculating past δ^2H_p based on δ^2H_{wax} measured in sediments, estimating ε_{app} is challenging because it varies both globally among plant growth forms and taxonomic groups (McInerney et al., 2011; Sachse et al., 2012), and locally among species growing at the same site (by up to ~100‰; Hou et al., 2007; Feakins and Sessions, 2010; Eley et al., 2014). Processes controlling ε_{app} in plants include evaporative ^2H-enrichment of plant source water during soil evaporation (McInerney et al., 2011) and leaf transpiration (Feakins and Sessions, 2010; Sachse et al., 2010; Kahmen et al., 2013a). In addition, biosynthetic ^2H-fractionation (ε_{bio}) during lipid production from intracellular water discriminates against ^2H, resulting in plant waxes that are D-depleted relative to plant source water (Sachse et al., 2012). ε_{bio} values can vary by 50 to 65‰ among species in natural settings and growth chambers (Kahmen et al., 2013a; Kahmen et al., 2013b). Field-based estimates of ε_{bio} in plants (based on leaf water and leaf wax δ^2H) show that ε_{bio} can also vary through the growing season within individual plants (Newberry et al., 2015; Freimuth et al., 2017; Tipple and Ehleringer, 2018), likely due to shifting

metabolic status (carbohydrate metabolism and carbon autonomy) of plants through phenological stages of growth (Cormier et al., 2018).

While much recent progress has been made in understanding the constituent controls on ε_{app} in modern plants, the process of lipid integration from plants to sediments is not as well understood (Sachse et al., 2012; Feakins et al., 2018). There is evidence that integration from the landscape can bias different plant-derived biomarkers toward different sources. Such bias may result from: differences among plant taxa, functional types or species in wax production (Diefendorf et al., 2011; Diefendorf et al., 2015) and δ^2H fractionation (Sachse et al., 2012; Gao et al., 2014); preferential degradation of functionalized lipid classes (e.g, *n*-alkanoic acids) in soils and sediments (Meyers and Ishiwatari, 1993); contrasting temporal and spatial averaging between functionalized lipids and *n*-alkanes in large river catchments (Hemingway et al., 2016); or over-representation of forested areas by lake sediment *n*-alkanes (Seki et al., 2010).

One of the main advantages of applying the δ^2H_{wax} proxy in lake sediments is that lakes can provide records of paleohydrologic conditions at exceptionally high temporal (~sub-decadal) and spatial (i.e., a single lake catchment) resolution (e.g., Feakins et al., 2014; Rach et al., 2014). The localized sensitivity of lacustrine δ^2H_{wax} records, however, can also make them vulnerable to inter-basin variability due to sourcing from vegetation assemblages unique to each lake catchment. For example, δ^2H_{wax} values can vary by as much as ~60‰ in the sediments of multiple lakes in close proximity as a result of differences in catchment vegetation or local aridity effects (Douglas et al., 2012; Daniels et al., 2017). It is therefore difficult to estimate ε_{app} with a high degree of confidence when reconstructing δ^2H_p using lake sediments.

The goals of this study were to 1) determine the variability in lake sediment δ^2H_{wax} in the absence of major differences in δ^2H_p among sites within the same region; 2) identify possible catchment-level drivers of site-to-site variability; and 3) compare the molecular and δ^2H composition of two plant wax compound classes (*n*-alkanes and *n*-alkanoic acids) to assess potential differences in their sourcing and ε_{app} values.

This study aims to identify catchment-level factors that can guide site selection to maximize the fidelity of δ^2H_{wax} to past δ^2H_p in lake sediments. Our approach was to survey δ^2H_{wax} in 12 lakes in the Adirondack Mountains, NY, USA that receive similar δ^2H_p but vary markedly in shoreline and catchment vegetation composition, lake to watershed area ratios, fluvial complexity and bulk sediment characteristics. Adirondack lakes have been the subject of comprehensive regional water quality monitoring (Driscoll and Newton, 1985; Driscoll et al., 1995) as well as several paleohydrological and paleovegetation studies (Charles et al., 1990; Whitehead et al., 1990; Stager et al., 2016).

2. Materials and methods

2.1. Sampling locations and sediment collection

This project focused on the Adirondack State Park, NY, USA (24,000 km^2; 37 to 1629 m above sea level), which has approximately 2,800 lakes covering 1,030 km^2, and 13,000 km of streams (Driscoll et al., 1991). The biome classification of the Adirondacks includes both cool mixed forest and temperate deciduous forest (Kaplan et al., 2003). The Adirondacks are a transitional vegetation zone between eastern deciduous angiosperm and mixed angiosperm-conifer forest with the distribution of vegetation assemblages dependent primarily on elevation. The Köppen-Geiger climate classification of the Adirondacks is humid continental (Peel et al., 2007). Thirty-year (1981-2010) normal climate data was obtained for each site from PRISM (2018). Annual mean data are reported for each site in Table 1 and EA1, monthly means are reported in Figure EA1. Across the 12 sites, mean annual temperature ranged from 4.9 to 6.2 ºC and precipitation from 1051 to 1207 mm/yr, with temperature minima in January and maxima in July (Fig. EA1). Monthly precipitation rates are generally lowest in February (55 to 71 mm) and highest in August (105 to 128 mm). These annual trends were similar to 30-year (1981-2010) observations obtained from the National Climatic Data Center (NCDC) for three stations in the

Adirondack Park (between 507 and 533 m asl). Across the Adirondack Park, precipitation amount generally increases from the northeast to the southwest, with the amount of spring precipitation dependent on latitude, and summer precipitation dependent primarily on elevation (Ito et al., 2002).

The sediment cores used in this study were collected from 12 lakes within the Adirondack Park (Fig. 1). All samples were collected on public lands designated as wilderness or wild forest areas, with the exception of Heart and Wolf lakes, which are privately owned by the Adirondack Mountain Club and the State University of New York, respectively. Details of the different sampling sites are reported in Table 1. The sampled lakes spanned elevations from 426 to 665 m asl and ranged in area from 0.1 to 7.5 km^2. A dam was built in 1923 at the north end of Chazy lake, and several logging dams were built along the Raquette river in the late 1800s. Sediment delivery and plant lipid sourcing may therefore not be comparable to other sites, which had smaller and less developed catchment areas (Table 1; Fig. 2). Based on data from the 2011 National Land Cover Database (NLCD; Homer et al., 2015), the 12 lake catchments are mostly (73 to 99%) forested, with varying proportions of evergreen and deciduous trees (Fig. 2a). The NLCD classifies forest cover based on leaf lifespan (i.e., evergreen and deciduous). In the Adirondacks, however, leaf lifespan is also an indicator of phylogeny because nearly all angiosperms are deciduous and gymnosperms are evergreen with the exception of deciduous conifers of the genus *Larix*, which are rare at the sites we sampled. Phylogeny is a major control on wax abundance in trees (Diefendorf et al., 2011; Diefendorf et al., 2015) and therefore we use both leaf lifespan and phylogeny when referring to the NLCD data for deciduous angiosperms (DA) and evergreen gymnosperms (EG). Using a 30 m shoreline buffer of the NLCD data around each lake, the 12 lake shorelines range from 7 to 79% EG coverage, with remaining vegetation including DA, mixed forest and woody wetlands (Fig. 2b).

Sediments were collected in October 2016 from an anchored boat and in January 2017 from lake ice. The upper ~1.0 meter of sediment was recovered from the deepest part of each lake (with the exception of Chazy and Raquette; Table 1) using a square-rod piston corer with a 1.5 m polycarbonate barrel (7 cm

diameter). An underwater camera was deployed to ensure that the sediment-water contact was captured during core recovery. Headspace water was drained and the polycarbonate tube was trimmed leaving a 2-5 cm void above the sediment. The void was filled with cellulose sponges (pre-cut to 7 cm diameter circles and pre-rinsed with deionized water) before capping tightly. Cores were transported and stored vertically at 4 °C until splitting and analysis.

A subset of the cores from Heart, Moose, Wolf, Debar, and East Pine were dated using ^{210}Pb by gamma counting at the Dartmouth GeoAnalytical Resource Center, Hanover, NH, USA. Based on these results, the age at 10 cm depth ranged from calendar year 1960 at Wolf lake to 2004 at Heart lake. We therefore estimate that the intervals used for plant wax analysis in this study (the upper 10 cm, see Section 2.3) represent approximately the last 50 yr, which is in good agreement with ^{210}Pb results from over 50 lakes throughout the Adirondacks (Binford, 1990; Binford et al., 1993).

2.2. Bulk sediment characterization

Each core was scanned for magnetic susceptibility using a Barington MS2 meter. Percent total organic matter and total carbonate were determined based on the mass loss-on-ignition (LOI) of 1 cm^3 aliquots of oven-dried sediment (60 °C overnight) after baking at 550 °C (4 h) and 1000 °C (2 h; Heiri et al., 2001). Approximately 1 cm^3 of sediment was taken from each core at 4, 8, and 12 cm and at 10 cm intervals from 20 cm to the base of the core for grain size analysis. Sample pre-treatment followed Gray et al. (2010) and Bird et al. (2014). Organic matter was removed using 30% H_2O_2 at room temperature for 24 h followed by three repeat 24 h treatments with 30% H_2O_2 in a 70 ºC water bath. Biogenic silica was removed using 1M NaOH at 60 ºC for 6 h. Lastly, carbonates were removed using 1M HCl at room temperature. Sediments were freeze dried and weighed to determine the percent lithics based on the mass loss after pretreatment. Grain size particle distribution was determined as an average of three measurements per sample using a Beckman-Coulter LS230 laser diffraction particle size analyzer.

An aliquot of each of the 36 samples of dried and homogenized sediment used for lipid extraction (see Section 2.3) was decarbonated (using 1M HCl until reaction completion, followed by DI water rinses until neutralized) and used to determine bulk sediment total organic carbon (TOC), total nitrogen (TN), and $\delta^{13}C_{org}$. Bulk $\delta^{13}C$ analyses were performed on decarbonated sediments, and on an aliquot of dried and homogenized plant leaves used for lipid extraction, via continuous flow (He; 120 ml/min) on a Costech elemental analyzer (EA) interfaced to a Thermo Electron Delta V Advantage IRMS via a Conflo IV. Raw $\delta^{13}C$ values were corrected for sample size dependency and normalized to the VPDB scale using a two-point calibration with in-house standards which were calibrated with IAEA standards (NBS-19, L-SVEC) to -38.26‰ and -11.35‰ VPDB following Coplen et al. (2006). Error was determined by analyzing two additional independent standards with a precision of 0.11‰ (1σ, n = 34) and accuracy of 0.09‰ (n = 34). Carbon/nitrogen (C/N) atomic ratios were determined from the molar ratios of TOC/TN.

2.3. Lipid extraction, separation and quantification

The uppermost sediments from each lake were subsampled at three 0.5 cm intervals (1.0 to 1.5, 5.0 to 5.5, and 9.0 to 9.5 cm depth) for a total of 36 samples, which were transferred to glass jars and freeze dried in preparation for lipid analysis. Three samples were taken from each core to gain additional insight into lipid variation over discrete depth and time intervals within the upper 10 cm, rather than taking a homogenized grab sample of surface sediment. Leaves were also collected for lipid analysis in May 2017 from DA (n = 13 individuals, 5 species) and EG plants (all conifers; n = 14 individuals, 7 species) at seven of the 12 sites where sediment was collected (Table 2). The same individual plants were simultaneously sampled for xylem water isotope analysis (see Section 2.5). Collection from a representative set of common terrestrial plant species was prioritized for comparison with recent sediments. Extensive terrestrial and aquatic plant surveys were beyond the scope of this study. Species-

level terrestrial and aquatic plant δ^2H_{wax} are therefore not comprehensively understood for the Adirondacks, but prior studies provide reference for temperate forested plant assemblages (Section 4).

The dry mass extracted for each individual sediment and plant sample is reported in Table EA1. Dried sediment was homogenized prior to accelerated solvent extraction (ASE; Dionex 350) with 9:1 (v/v) DCM/MeOH using three extraction cycles at 100 ºC and 10.3 MPa. Approximately 200 mg of powdered leaves from each plant was extracted by sonicating twice with 20 ml of DCM/MeOH (2:1, v/v), centrifuging and pipetting the lipid extract into a separate vial after each round of sonication. For both sediment and leaves, the total lipid extract was saponified with 3 ml of 0.5 N KOH in MeOH/H_2O (3:1, v/v) for 2 h at 75 ºC. Once cool, 2.5 ml of NaCl in water (5%, w/w) was added and then acidified with 6N HCl. The solution was extracted with hexanes/DCM (4:1, v/v), neutralized with $NaHCO_3$/H_2O (5%, w/w), and water was removed through addition of Na_2SO_4. Neutral and acid fractions were separated using DCM/IPA (2:1, v/v) and 4% formic acid in diethyl ether, respectively, over aminopropyl-bonded silica gel. The neutral fraction was then separated into aliphatic and polar fractions using activated alumina oxide column chromatography. The aliphatic fraction was separated over 5% silver nitrate silica gel with hexanes to collect saturated compounds. The acid fraction was evaporated under a gentle stream of nitrogen and methylated by adding ~1.5 ml of 95:5 MeOH/12 N HCl (v/v) of known δ^2H composition and heating at 70 ºC for 12-18 h. HPLC grade water was then added and the methylated acid fraction was extracted with hexanes and eluted through Na_2SO_4 to remove water before separation over 5% deactivated silica gel with DCM to collect fatty acid methyl esters (FAMEs).

n-Alkanes and FAMEs were identified by gas chromatography–mass spectrometry (GC-MS) using an Agilent 7890A GC and Agilent 5975C quadrupole mass selective detector system, and quantified using a flame ionization detector (FID). Compounds were separated on a fused silica column (Agilent J&W DB-5ms; 30 m x 0.25 mm, 25 µm film) and the oven ramped from an initial temperature of 60 ºC (held 1 min) to 320 ºC (held 15 min) at 6 ºC/min. Compounds were identified using authentic standards, fragmentation

patterns and retention times. All samples were diluted in hexanes spiked with 1,1'-binaphthyl as an internal standard prior to quantification. Compound peak areas were normalized to those of 1,1'-binaphthyl and converted to concentration using response curves for an in-house mix of *n*-alkanes (even-chains from C_{14} to C_{18}; odd-chains from C_{25} to C_{35}) and FAMEs (C_{16}, C_{18}, C_{24}, C_{28}, C_{30}) at concentrations ranging from 0.5 to 100 µg/ml. Precision and accuracy were determined by analyzing external standards at 25 µg/ml as unknowns and were 0.61 (1σ, n = 13) and 0.41 (1σ, n = 13), respectively. Quantified concentrations were normalized to the mass of dry sediment or leaf material extracted and to the equivalent mass of TOC extracted. Recovery standards were not used and therefore we cannot account for potential loss of lipids during lipid extraction and separation steps. FAME concentrations were converted to equivalent *n*-alkanoic acid concentrations using respective molar masses.

Average chain length (ACL) is the weighted average concentration of all the long-chain waxes, defined as

$$\mathrm{ACL}_{a-b} = \sum_{i=a}^{b} \frac{i[Ci]}{[Ci]} \quad \text{(Eq. 1)}$$

where *a*-*b* is the range of chain lengths and C_i is the concentration of each wax compound with *i* carbon atoms. $ACL_{27\text{-}35}$ is used to indicate ACL values for *n*-C_{27} to *n*-C_{35} alkanes (odd chain-lengths only). $ACL_{26\text{-}30}$ is used to indicate ACL values for *n*-C_{26} to *n*-C_{30} alkanoic acids (even chain-lengths only). The carbon preference index (CPI) for *n*-alkanes is defined as

$$CPI_{alk} = \left[\sum C_{23-33} + \sum C_{25-35}\right] / \left(2 * \sum C_{24-34}\right) \quad \text{(Eq. 2)}$$

where the numerator (denominator) includes only odd (even) chain-lengths, following Marzi et al. (1993). The CPI for *n*-alkanoic acids is defined as

$$CPI_{acid} = \left[\sum C_{22-28} + \sum C_{24-30}\right] / \left(2 * \sum C_{23-29}\right) \quad \text{(Eq. 3)}$$

where the numerator (denominator) includes only even (odd) chain-lengths, following and Feakins et al. (2018). We note that CPI is here defined to include mid-chain lengths (*n*-$C_{22\text{-}26}$) that are not specific to terrestrial plants. Following Bush and McInerney (2013), sedimentary CPI_{alk} values > 2 are interpreted as

a qualitative indicator for a predominance of odd *n*-alkane or even *n*-alkanoic acid chain-lengths typical in modern plants and thermally immature sediments.

2.4. δ^2H analysis of n-alkanes and n-alkanoic acids

The δ^2H composition of *n*-alkanes (sediments and plants) and *n*-alkanoic acids (sediments only; plant fatty acid fractions had insufficient peak separation for compound-specific isotope analysis) was determined using a Thermo Trace GC Ultra coupled to an Isolink pyrolysis reactor (1420 ºC) and interfaced to a Thermo Electron Delta V Advantage IRMS via a Conflo IV. The GC oven program ramped from 80 ºC (held 2 min) to 320 ºC (held 15 min) at a rate of 8 ºC/min. The H_3^+ factor was tested daily and averaged 4.8 ppm/nA during the period of analysis. Data were normalized to the VSMOW/SLAP scale using a standard *n*-alkane mix of known δ^2H composition (Mix A5; A. Schimmelmann, Indiana University). The long-term precision of a co-injected *n*-C_{38} alkane standard was 2.9‰ (1σ, n = 40). The δ^2H value of hydrogen added to *n*-alkanoic acids during derivatization was determined by mass balance of phthalic acid of known δ^2H composition (A. Schimmelmann, Indiana University) and derivatized methyl phthalate (Polissar and D'Andrea, 2014). Hydrogen isotopic fractionations are reported as epsilon values (in units of per mil, ‰), using the following equation:

$$\varepsilon_{a-b} = \left[\frac{(\delta D_a + 1)}{(\delta D_b + 1)}\right] - 1 \quad \text{(Eq. 4)}$$

where *a* is the product and *b* is the substrate. All epsilon values herein are interpreted based on their absolute values (e.g., larger ε_{app} means that the absolute value of ε_{app} is greater).

2.5. Water sampling and isotope analysis

Surface water samples were collected from lakes and rivers throughout the Adirondacks in July and October 2016 and January and May 2017 using 30 ml Nalgene bottles. At the time of sampling, water

temperature and conductivity were measured and the sampling location was determined using GPS. Surface water δ^2H and $\delta^{18}O$ values were measured at Indiana University-Purdue University Indianapolis (IUPUI) with a Picarro L2130-i Analyzer and normalized to the VSMOW scale following the method of van Geldern and Barth (2012) using Los Gatos and USGS standards. Precision and accuracy based on replicate analyses of three previously calibrated in-house standards were 0.6‰ and 1.3‰ respectively, for δ^2H, and 0.05‰ and 0.15‰, respectively, for $\delta^{18}O$.

Plant material for xylem water isotope analysis was collected in May 2017 from DA (n = 13 individuals, 5 species) and EG plants (all conifers; n = 14 individuals, 7 species) at seven of the 12 sites where sediment was collected (Table 2). Plant sampling methods followed Freimuth et al. (2017). Briefly, two stems (<1.0 cm diameter) were clipped from each individual, stripped of outer bark, and sealed in separate pre-ashed glass exetainer vials with airtight septa screwcaps. Each sample was treated and analyzed separately. All samples were kept in a cooler in the field and frozen (-5 ºC) in the lab until water extraction.

Xylem water was extracted using cryogenic vacuum distillation following West et al. (2006). Exetainer vials containing frozen stems were evacuated to a pressure <8 Pa (<60 mTorr), isolated from the vacuum pump, and heated to 100 ºC. Water vapor was collected in borosilicate test tubes immersed in liquid nitrogen for a minimum of 60 minutes. To verify extraction completion, samples were weighed following cryogenic vacuum distillation and then again after freeze drying. Based on the mass difference, the recovery of xylem water was >99%. Collected water was thawed and pipetted into 2 ml crimp-top vials and refrigerated at 4 ºC until analysis.

Analysis of xylem water $\delta^{18}O$ and δ^2H was made by headspace equilibration. For $\delta^{18}O$ analysis, 500 µl of water was transferred to an exetainer vial, stoppered, and purged using an offline purging manifold system with 0.3% CO_2 in He for 10 minutes at 120 ml/min (Paul and Skrzypek, 2006). Samples were then

equilibrated in a water bath at 25ºC for 18 hours. For δ^2H analysis, 200 µl of water was transferred to an exetainer vial, and a Pt catalyst was added. Samples were purged using 2% H_2 in He for 10 minutes at 120 ml/min and equilibrated at 25ºC for 1 hour. The isotopic composition of equilibrated headspace gases was analyzed on a Thermo Delta V Advantage IRMS with a Thermo Gasbench II connected to the IRMS via a Conflo IV interface. For δ^2H analysis, volatile organics were removed from the sampled headspace gas by passing the capillary through a liquid nitrogen trap before isotope analysis. Data were normalized to the VSMOW/SLAP scale (Coplen, 1988) using three in-house standards. For xylem waters, precision and accuracy were 1.6‰ (1σ, n = 20) and 2.5 ‰ (n = 20), respectively, for δ^2H and 0.3‰ (1σ, n = 22) and -0.1‰ (n = 22), respectively, for $\delta^{18}O$.

We calculated deuterium excess (*d*-excess) as a measure of the extent of evaporation affecting the isotopic composition of each water sample using the following equation (Dansgaard, 1964):

$$d\text{-excess} = \delta^2H - 8 * \delta^{18}O \quad \text{(Eq. 5)}$$

The average *d*-excess value for precipitation is 10‰. As environmental waters undergo evaporation (kinetic fractionation), *d*-excess values typically decrease to values below 10‰ (Clark and Fritz, 1997). Data reduction and analysis was completed using JMP Pro 12.0 (SAS, Cary, USA) and we assign significance for alpha levels at or below 0.05. Mean values are presented with ± 1 standard deviation.

3. Results

3.1. Bulk sediment characteristics

The average total organic matter (%TOM) determined by loss-on-ignition from the upper 50 cm of sediment ranged from 14 to 68% among all 12 sites, with most sites between 20 to 40%. The total carbonate (%TC) was less than 6% in all cores. Magnetic susceptibility was consistently low (< 5.3 SI units) across all cores. Grain size distributions in the upper 50 cm of sediments varied widely, with most sites dominated by clay or silt (Electronic Annex Table EA1).

The C/N ratios of individual leaf and sediment samples are reported in Table EA1. The C/N ratios of plant leaves ranged from 15 to 74, with a lower mean for DA (25) and EG plants (60). Mean sediment C/N ratios in each lake ranged from 12 to 16 (Table 1). These values are intermediate between typical C/N ratios for lake algae (4-10) and vascular land plants (> 20; Meyers, 2003). Across all sites, we observed a 25% range in TOC (from 10% at Chazy to 35% at Quiver), and a ~5‰ range in $\delta^{13}C_{org}$ (from -31.9‰ at Quiver to -26.8‰ at Chazy; Table 1). There was an inverse relationship between TOC and $\delta^{13}C_{org}$ values among lakes ($R^2 = 0.42$, $p < 0.0001$; Fig. 3). Particularly low $\delta^{13}C_{org}$ at several sites (< -30‰; Fig. 3) may reflect either reduced algal productivity or incorporation of ^{13}C-depleted DIC from the heterotrophic respiration of sedimentary organic matter (Meyers, 2003; Diefendorf et al., 2008). Lower TOC in Chazy and Raquette lakes, which are dammed, may reflect an apparent dilution of organics with relatively high sand and silt in the sediment grain size distribution at those sites (Table EA1).

3.2. Adirondack isotope hydrology

3.2.1. Surface and meteoric water isotopes

Adirondack lake waters sampled between July 2016 and May 2017 had δ^2H values ranging from -81 to -42‰ and $\delta^{18}O$ values from -11.9 to -5.0‰ (Fig. 4 and EA2; Table EA3). The mean isotope values of lakes varied by season, with more positive values in July and October 2016 (δ^2H, -62 and -57‰; $\delta^{18}O$, -8.1 and -7.3‰, respectively) and more negative values in January and May 2017 (δ^2H, -65 and -68‰;

$\delta^{18}O$, -8.9 and -9.4‰, respectively; Figure EA2). Lake waters sampled in this study were comparable to those reported for different Adirondack lakes sampled in September 2007 (-69‰, $\delta^{2}H$ and -9.2‰, $\delta^{18}O$; Brooks et al., 2014; Figure EA2). There was a significant ^{2}H- and ^{18}O-enrichment of lake water in basins with no fluvial inlets relative to basins with one or more inlets in July, October and May (t-test, $p \leq 0.03$ and 0.007, respectively) but not in January. The overall mean *d*-excess value for Adirondack lakes in this study was 3.8 ± 4.4‰ (n = 75), in agreement with mean *d*-excess values measured by Brooks et al. (2014) from Adirondack lakes in September (4.7‰; Fig. EA3). Lake water *d*-excess values were significantly lower in basins with no fluvial inputs (1.6 ± 2.7‰, n = 34) than in basins with one or more inlets (5.9 ± 4.3‰, n = 39; t-test, $p < 0.0001$). Lake water *d*-excess values were also lower in the summer and autumn (2.5‰ in July and 1.9‰ in October) than in winter and spring (6.2‰ in January and 6.7‰ in May). These values indicate that Adirondack lakes undergo significant evaporation (kinetic fractionation), especially for basins with no fluvial inputs and during summer months.

River waters sampled in July and October ranged from -78 to -52‰ for $\delta^{2}H$ and from -11.4 to -8.2‰ for $\delta^{18}O$, overlapping with lake water values across all seasons (Fig. 4 and EA2). Rivers sampled in this project (n = 9) and in the 1980s within 60 km of Adirondack Park (Kendall and Coplen, 2001; August through October, n = 34) had nearly identical mean $\delta^{2}H$ (-64‰ and -66‰, respectively) and $\delta^{18}O$ (-9.2‰ and -9.4‰, respectively) values. The mean *d*-excess value from rivers (9.8‰) was close to the expected value for meteoric water (10‰), and significantly higher than lakes (3.8‰; $p = 0.0002$; Fig. EA3). This suggests that, consistent with a synoptic survey of rivers throughout the conterminous USA (Kendall and Coplen, 2001), rivers in the Adirondacks integrate the $\delta^{18}O$ and $\delta^{2}H$ values of meteoric waters and are a reliable surface water proxy for regional meteoric water.

The regional evaporation line (REL; based on all Adirondack lake water isotopes) intercepts the RMWL (based on precipitation collected since 1972 at the GNIP station in Ottawa ~100 km northwest of the

Adirondack Park; IAEA/WMO, 2018), at a δ^2H value of -75‰ and a $\delta^{18}O$ value of -10.8‰ (Fig. 4). This provides an estimate of the isotope composition of mean annual precipitation (MAP) in the sampled Adirondack region, and is in close agreement with the weighted MAP values from GNIP Ottawa data of -76‰ for δ^2H_{MAP} and -11.0‰ for $\delta^{18}O_{MAP}$ (IAEA/WMO, 2018). The intercept of the REL with meteoric water lines based on precipitation collected approximately 160 km southwest of the Adirondack Park in Tompkins County, NY (δ^2H, -78‰ and $\delta^{18}O$, 11.3‰; Coplen and Huang, 2000) and based on modeled precipitation from the Online Isotopes in Precipitation Calculator (OIPC) for the 12 Adirondack lake sites (δ^2H, -77‰, and $\delta^{18}O$, -11.1‰; Bowen and Revenaugh, 2003; IAEA/WMO, 2015; Bowen, 2017; Bowen et al., 2005) were similar to that based on the GNIP data. Therefore, we use the intercept of Adirondack lake waters with the OIPC-based meteoric water line to estimate δ^2H_{MAP} (-77‰) and $\delta^{18}O_{MAP}$ (-11.1‰) for the sampled region, which is also similar to comparable estimates from lakes sampled by Brooks et al. (2014; -76‰) and nearby rivers sampled by Kendall and Coplen (2001; -73‰).

3.2.2. Plant water isotopes

Xylem water δ^2H values (δ^2H_{xw}) collected in May 2017 ranged from -89 to -60‰ with an overall mean of -76 ± 6‰ (n = 43; Fig. 4 and EA2; Table EA3), similar to δ^2H_{MAP} estimates from the intercept of the Adirondack lake REL with RMWLs in Section 3.2.1 (-75 to -78‰). Mean δ^2H_{xw} values were not significantly different among sites (ANOVA, $p = 0.07$) or between deciduous angiosperms (-77‰) and evergreen gymnosperms (-74‰; t-test, $p = 0.05$). Xylem water *d*-excess ranged from -4.6 to 16.2‰, with a mean of 4.8‰ (Fig. EA3), indicating that some plant waters were evaporatively enriched (*d*-excess < 10‰) while others were not. For comparison, May/June precipitation at Ottawa from 2007-2017 had *d*-excess values of 9.7‰. Xylem *d*-excess values in angiosperms (3.1 ± 4.4‰, n = 17) were modestly but significantly (t-test, $p = 0.018$) lower than in gymnosperms (6.8 ± 4.7‰, n = 21). Greater evaporative enrichment of angiosperm source waters may reflect differences in leaf lifespans, rooting structure or

hydraulic anatomy and freeze-thaw cavitation resistance between angiosperm xylem vessels and gymnosperm tracheids (Brodribb et al., 2012). Additionally, groundwater contributions to gymnosperms and angiosperms may differ, although this may depend on site-specific conditions (Evaristo et al., 2017; Evaristo and McDonnell, 2017).

3.3. Plant wax abundance and distribution

Molecular distributions for lake sediment *n*-alkanes and *n*-alkanoic acids are summarized in Table 3 and Fig. 5 and 6. Comparable data for plants are reported in Table 2. All molecular data for individual plant and sediment samples are reported in Table EA1. All lake sediments had detectable amounts of *n*-C_{16} to *n*-C_{30} alkanoic acids and *n*-C_{17} to *n*-C_{35} alkanes. In sediments, total long-chain (*n*-C_{27} to *n*-C_{35}) alkane concentrations were similar across all sites (191 ± 53 µg/g TOC) while total long-chain (*n*-C_{28} and *n*-C_{30}) alkanoic acid concentrations were considerably more variable (117 ± 116 µg/g TOC; Fig. 6). In plants, DA trees produced significantly more total long-chain *n*-alkanes than EG trees (471 and 33 µg/g TOC, respectively; Fig. 6), while total long-chain *n*-alkanoic acid concentrations were comparable for DA and EG trees (15 and 20 µg/g TOC, respectively). There were large species-level differences in leaf wax concentration and distribution. For example, the evergreen *Thuja occidentalis* produced over two orders of magnitude more *n*-C_{35} alkane than any other species (Table EA1).

In sediments, the long-chain (≥*n*-C_{27}) compounds in highest abundance (C_{max}) were generally *n*-C_{28} alkanoic acids and *n*-C_{29} alkanes (Fig. 6). The dominance of *n*-C_{29} alkane was reflected in mean sediment $ACL_{27\text{-}35}$ (29.5 ± 0.2, n = 36), which had similar values but higher variability in DA (28.8 ± 1.2, n = 13) and EG (30.0 ± 2.5, n = 14) plants. We note that for several lakes, the distribution of the entire range of *n*-C_{17} to *n*-C_{35} alkanes was dominated by mid-chain lengths (specifically, *n*-C_{21} and *n*-C_{23} alkanes; Fig. 5), distributions typically associated with submerged and floating aquatic plant sources (Ficken et al., 2000).

While there is evidence that trees are a dominant source of sedimentary long-chain *n*-alkanes for lakes in temperate forested catchments (Seki et al., 2010; Freimuth et al., 2019), certain aquatic plant species can also produce long-chain (≥*n*-C_{27}) alkanes as well (Aichner et al., 2010; Liu and Liu, 2016). Given that aquatic plants were not sampled in this study we cannot directly assess the lipid distributions of the local aquatic sources and further work is needed to constrain the contribution of aquatic plants to Adirondack lake sediments.

For *n*-alkanoic acids, the mean $ACL_{26\text{-}30}$ was similar for sediments (26.5 ± 0.07) and DA plants (26.6 ± 0.3, n = 12) but higher in EG plants (27.6 ± 0.6, n = 14), which reflects significantly higher *n*-C_{30} to *n*-C_{28} acid concentration ratios in EG plants (3.6) than in DA plants or sediments (0.3 and 0.5, respectively; Fig. 6). Most lakes had long-chain *n*-alkane concentrations that were either higher than or comparable to long-chain *n*-alkanoic acid concentrations, with four exceptions (Chazy, East Pine, Little Green, and Hope; Fig. 6).

The overall mean CPI_{acid} was similar between lake sediments (3.0 ± 0.6, n = 36) and modern plants pooled by species (3.8 ± 1.2, n = 10 species, 24 individuals; Table 3). For *n*-alkanes, the overall mean CPI_{alk} was lower and less variable for lake sediments (2.6 ± 0.9, n = 36) than for terrestrial plants (6.1 ± 5.8, n = 12 species, 27 individuals; Table 3). Low CPI_{alk} (< ~2) in thermally immature sediments can reflect degradation (though we did not observe a significant change in CPI_{alk} with depth), petrogenic aerosols from gasoline and diesel (though these contain few *n*-alkanes > *n*-C_{27} (Bai et al., 2014), which are the main focus of this study), or microbial or algal sources (Freeman and Pancost, 2014). We note that CPI_{alk} is highly variable in terrestrial plants and therefore following recommendations from a systematic meta-analysis (Bush and McInerney, 2013), we interpret sedimentary CPI_{alk} values at or above a threshold of 2 as a qualitative indicator of terrestrial plant sources. CPI_{alk} ranged from 1.9 to 5.8 in Adirondack

sediments (and from 1.3 to 32 in Adirondack plants), which is therefore qualitatively consistent with terrestrial plant sources; we consider the potential influence of additional sources further in Section 4.

3.4. Plant wax δ^2H and ε_{app} values

Sedimentary δ^2H_{wax} data are reported in Table 3 and Fig. 7. All isotopic data for individual plant and sediment samples are reported in Table EA1. The mean *n*-C_{28} and *n*-C_{30} alkanoic acid δ^2H values in the upper 9 cm of sediment across all sites were -164 ± 9‰ and -159 ± 9‰, respectively. *n*-Alkanes were significantly D-depleted relative to *n*-alkanoic acids across all long-chain homologues (mean *n*-C_{27}, *n*-C_{29} and *n*-C_{31} alkane δ^2H were -191 ± 7‰, -188 ± 6‰ and -176 ± 6‰, respectively; *t*-test, $p < 0.0001$ for pairwise comparisons between each long-chain *n*-alkane and *n*-alkanoic acid). The overall δ^2H_{wax} variability was significantly larger for *n*-C_{28} alkanoic acid (1σ = 9‰, n = 34) than for *n*-C_{29} alkane (1σ = 6‰; Levene test, $p = 0.004$; Fig. 7). There were significant differences in δ^2H_{wax} values among lakes, for both *n*-C_{28} alkanoic acid (Kruskal-Wallis test, H = 30, 11 d.f., $p = 0.0014$) and *n*-C_{29} alkane (Kruskal-Wallis test, H = 31, 11 d.f., $p = 0.0012$). In plants, the pooled mean *n*-C_{27}, *n*-C_{29} and *n*-C_{31} alkane δ^2H values across all species were -156 ± 11‰, -175 ± 14‰ and -174 ± 17‰, respectively. We note that mean *n*-C_{27} and *n*-C_{29} alkane δ^2H_{wax} values were significantly higher in plants than in sediments (*t*-test, $p < 0.0001$), while *n*-C_{31} alkane δ^2H_{wax} was not significantly different (*t*-test, $p = 0.6$). There was no significant difference between the pooled mean *n*-alkane δ^2H_{wax} values of DA and EG plants (*t*-test, p = 0.4 to 1.0 across long-chain *n*-alkane homologues).

Within the *n*-alkane class, the δ^2H of long-chain homologues in sediments were positively correlated with one another and had significant shared variance (*n*-C_{29} with *n*-C_{27} and *n*-C_{31}, R^2 = 0.63 and 0.38, respectively, $p < 0.0001$ for both). Stronger shared variance for *n*-C_{29} and *n*-C_{27} alkanes suggests that

these two compounds likely have a similar water source, while *n*-C_{31} may either reflect different source water δ^2H or derive from different plant sources as suggested by Garcin et al. (2012) in the West African tropics. By contrast, in plants there was no relationship between *n*-C_{27} and *n*-C_{29} alkanes ($R^2 = 0.064$, $p = 0.2578$), while *n*-C_{29} and *n*-C_{31} alkanes had greater shared variance than in sediments ($R^2 = 0.716$, $p < 0.0001$). The δ^2H of long-chain *n*-alkanoic acid homologues in sediments were positively correlated with shared variance indicating common biological or environmental influences (*n*-C_{28} with *n*-C_{26} and *n*-C_{30}, $R^2 = 0.53$ and 0.67, respectively, $p < 0.0001$ for both).

Comparing between compound classes, *n*-alkanoic acid and *n*-alkane δ^2H values were not significantly correlated with one another for all long-chain homologues except *n*-C_{27} alkane and *n*-C_{30} acid ($p = 0.02$). This indicates that, while controls on δ^2H_{wax} are largely shared within compound classes, there are distinct controls on *n*-alkanes and *n*-alkanoic acids. The weighted mean δ^2H values for *n*-alkanes (*n*-C_{27} to *n*-C_{31}) and *n*-alkanoic acids (*n*-C_{28} to *n*-C_{30}) are within 1-2‰ of the values for *n*-C_{29} alkane and *n*-C_{28} acid due to the dominance of these homologues (Fig. 6). The discussion section is focused on individual homologues (primarily *n*-C_{29} alkane and *n*-C_{28} alkanoic acid) as well as the δ^2H differences between long-chain *n*-C_n alkanes and their biosynthetic precursor *n*-C_{n+1} alkanoic acids.

Within individual lakes, *n*-alkane δ^2H was always more negative than *n*-alkanoic acid δ^2H, but the magnitude of the δ^2H offset between homologues varied among sites (Fig. 7). The δ^2H offset between *n*-C_{29} alkane and *n*-C_{30} acid ($\varepsilon_{C29\text{-}C30}$) ranged from -8‰ (Raquette) to -58‰ (Little Green; Fig. 8), and offsets between *n*-C_{27} alkane and *n*-C_{28} acid ($\varepsilon_{C27\text{-}C28}$) were comparable. Across all sites, mean $\varepsilon_{C29\text{-}C30}$ was -35‰ and $\varepsilon_{C27\text{-}C28}$ was -33‰ (Table 3), similar in sign and magnitude to (but more variable than) that observed previously in temperate plants (-20 to -30‰; Chikaraishi and Naraoka, 2007; Hou et al., 2007; Freimuth et al., 2017).

Lastly, we determined ε_{app} values based on various source water estimates (Table 3). First, based on mean xylem water (δ^2H_{xw} = -76‰), which was within 1‰ of our regional δ^2H_{MAP} estimate (-77‰; Section 3.2.1) we determined ε_{app} for sedimentary *n*-C_{29} alkane ($\varepsilon_{C29\text{-}xw}$; -122 ± 6‰, n = 36) and *n*-C_{28} alkanoic acid ($\varepsilon_{C28\text{-}xw}$; -95 ± 10‰, n = 34). We also determined ε_{app} based on OIPC-modeled δ^2H_{MAP} at each site (-76 to -72‰) for *n*-C_{29} alkane ($\varepsilon_{C29\text{-}MAP}$; -123 ± 6‰, n = 36) and *n*-C_{28} alkanoic acid ($\varepsilon_{C28\text{-}MAP}$; -97 ± 9‰, n = 34). Mean plant ε_{app} values for *n*-C_{29} alkane were similar when calculated based on xylem water ($\varepsilon_{C29\text{-}xw}$) and on OIPC-modeled δ^2H_{MAP} ($\varepsilon_{C29\text{-}MAP}$), ranging from -106 to -109‰ at each site (Table 3).

4. Discussion

4.1. Basin-scale drivers of sedimentary n-alkyl lipid composition

Sedimentary *n*-alkane concentrations were remarkably consistent across the 12 sampled lakes, but long-chain *n*-alkanoic acid concentrations varied widely (Fig. 6). This suggests that long-chain *n*-alkane concentrations in sediments are relatively insensitive to basin-scale differences in terrestrial plant assemblage and wax production, whereas the opposite is true for *n*-alkanoic acids. In addition, the total range in sedimentary *n*-alkane and *n*-alkanoic acid δ^2H (22‰ and 35‰, respectively) was larger than we would expect based on estimated differences in δ^2H_{MAP} among sites (~4‰, Fig. 4). Here, we assess the potential influence of basin-scale factors (specifically, vegetation assemblage and local aridity) on the observed variability in wax distributions and δ^2H_{wax} values in lake sediments.

4.1.1. Influence of basin-scale vegetation on sedimentary n-alkyl lipids

All of the lake basins in this survey are forested, but the mix of plant types (especially DA and EG abundance) varies considerably (Fig. 2) which could lead to differences in wax abundance and distribution, biosynthetic δ^2H fractionation, and timing of wax synthesis in the source vegetation contributing to the sediments in each basin. While a species-level plant survey of each catchment was beyond the scope of this study, we used the 2011 NLCD data to characterize the distribution of major plant types at the basin-level. This land cover data cannot account for differences in leaf wax production rates among plant taxa, growth forms or species, but can provide insight into whether the mix of DA and EG plants at each site influences sedimentary plant lipid distributions (e.g., Giri et al., 2015). In particular, the abundance ratio of long-chain (*n*-C_{27} to *n*-C_{35}) alkanes to long-chain (*n*-C_{28} and *n*-C_{30}) acids in sediments varied widely among sites (0.5 to 7.4; Fig. 6; Table 3), and was negatively correlated with the abundance of EG plants (Fig. 9) in each lake catchment and in a 30 m buffer around the shoreline of each lake (R^2 = 0.37 to 0.41, respectively, $p < 0.0001$). When Chazy and Raquette are excluded from this analysis due to the potential influence of damming on organic matter sourcing and shoreline flooding (Section 2.1), the strength of the relationship increases further (R^2 = 0.52 to 0.67, $p < 0.0001$; Fig. 9). This suggests that sedimentary waxes are sensitive to local plant assemblages at the catchment- or shoreline-scale. EG plants in particular may be an important source of long-chain fatty acids at sites with more than ~40% EG plant cover (Fig. 9). This is consistent with observations that DA plants had significantly higher mean *n*-$C_{27\text{-}35}$ alkane to *n*-$C_{28\text{-}30}$ acid ratios (32) than EG plants (4) and sediments (3; Table 2). Further, CPI_{acid} values were similar for sediments and EG plants (3.0 and 3.0) but slightly higher in DA plants (5.0), providing additional supporting evidence for EG-derived *n*-alkanoic acids in sediments.

Phylogeny is a major control on the relative abundance of *n*-alkyl lipids in conifers, and while *n*-alkanoic acids are generally less abundant than *n*-alkanes at the family level (Diefendorf et al., 2015), this broad trend can vary among specific families and species. One such exception is the Pinaceae family, which is well represented among common Adirondack EG species. For example, five of the seven EG species we sampled (including the genera *Tsuga, Pinus, Picea* and *Abies*) are in the Pinaceae family and had a higher

abundance of *n*-C_{28-30} alkanoic acids than *n*-C_{27-35} alkanes (Table 2), which could contribute to the similar *n*-alkane to *n*-acid ratios in EG plants and sediments (Table 2 and 3). Major trends in wax production among plant functional types (e.g., DA, EG) are important guides for interpreting possible sources of sedimentary *n*-alkyl lipids, but these trends can vary with greater phylogenetic specificity (Diefendorf et al., 2011, 2015). Therefore, constraining the composition of source vegetation at the family- or species-level using pollen or macrofossil data can provide important insight into wax sources.

EG plant abundance in lake catchments and shorelines was closely related to the relative abundance of *n*-alkanoic acids and *n*-alkanes in sediments, but it had no significant relationship to sediment ε_{app} (*p*-value > 0.8 for both $\varepsilon_{C28\text{-}MAP}$ and $\varepsilon_{C29\text{-}MAP}$). This is in contrast to a prior study that found that the composition of catchment vegetation could explain between 28% and 70% of the variability in sedimentary ε_{app} from adjacent lakes, depending on the *n*-alkane or *n*-alkanoic acid homologue (Daniels et al., 2017). However, that study took place in an Arctic tundra biome where watersheds were distinguished by the dominance of either grasses or shrubs, reflecting major ε_{app} differences between monocots and eudicots (Sachse et al., 2012). By contrast, the Adirondack lake catchments in this study are all forested and distinguished instead by the proportion of either DA or EG trees, which had no significant difference in $\varepsilon_{C29\text{-}MAP}$ (*t*-test, $p = 0.98$; Table 2). Prior studies have generally not found any systematic differences in ε_{app} between gymnosperms and angiosperms growing in the same environment (Chikaraishi and Naraoka, 2003; Bi et al., 2005; Gao et al., 2014). One exception is a study that found distinctly larger ε_{app} in evergreen conifers than in coexisting deciduous angiosperms (Pedentchouk et al., 2008), however that was in a semi-desert setting and may therefore not be applicable to the cold/continental climate and mixed EG/DA forest structure of the Adirondacks. We would therefore not necessarily expect EG vegetation cover to impact sediment ε_{app}.

We did find that wetland cover (including woody wetlands and emergent aquatic plants) was negatively correlated with sedimentary *n*-C_{28} and *n*-C_{30} acid δ^2H_{wax} values ($R^2 = 0.43$ and 0.49, respectively, $p <$

0.0001). The extent of wetland cover is small (accounting for between 0 and 7% of total catchment area), but nevertheless the basins with more wetland coverage had larger *n*-alkanoic acid ε_{app} values. The negative correlation may reflect the use of evaporatively ^{2}H-enriched lake water or other surface waters by wetland vegetation compared to the use of soil water by trees. Meanwhile, *n*-C_{29} and *n*-C_{31} alkane ε_{app} had no relationship with the abundance of wetland cover (p = 0.3 to 0.5). This may further indicate distinct plant sources (possibly accessing different water pools) for long-chain *n*-alkanes and *n*-alkanoic acids, which is explored further in Section 4.3.

4.1.2. Influence of basin-scale aridity on sedimentary n-alkyl lipids

We examined the relationship between sedimentary wax ε_{app} and the evaporative ^{2}H- and ^{18}O-enrichment of lake water, which has been previously established as an indicator of local (basin-scale) aridity (Polissar and Freeman, 2010). The evaporative enrichment of lake water relative to mean annual precipitation ($\varepsilon_{lw\text{-}MAP}$) has two main drivers: 1) climatic factors (including relative humidity, temperature, precipitation/evaporation ratios, and the isotopic composition of meteoric water) and 2) lake water balance (the net flux and isotopic composition of total inflows from precipitation, surface water and groundwater and total outflows from surface and ground waters and evaporation; Gat, 1995; Gibson and Edwards, 2002; Polissar and Freeman, 2010). The climatic factors influencing lake water evaporative ^{2}H- and ^{18}O-enrichment also affect soil and plant water ^{2}H- and ^{18}O-enrichment. $\varepsilon_{lw\text{-}MAP}$ can therefore be used to investigate possible climatic drivers of plant wax $\delta^{2}H$ differences among sites. Before we assess climatic drivers of lake and plant water ^{2}H-enrichment, we must also assess the effect of lake water balance. Performing a comprehensive water budget analysis including seasonal surface and ground water discharge for each lake was beyond the scope of this study. Instead we use the lake/catchment area ratio of each basin to approximate the ratio of lake evaporation to watershed runoff (e.g., Polissar and Freeman, 2010).

The 12 lakes in this study had $\varepsilon_{lw\text{-}MAP}$ values ranging from 0.4 to 5.4‰ (Table 1), and we found no relationship between $\varepsilon_{lw\text{-}MAP}$ (based on OIPC-modeled $\delta^{18}O_{MAP}$ and the mean measured lake water $\delta^{18}O$ values at each site) and lake/catchment area ratio ($R^2 = 0.05$, $p = 0.18$). Seasonality can also have a strong impact on evaporative enrichment of surface waters (Gibson et al., 2008), but surface water data suggests this is not a major factor in the Adirondacks. The Adirondack REL has a slope of 5.1 which is typical for lake water evaporation lines in mid-latitude climates that lack strong precipitation seasonality (≤5; Gibson et al., 2008) and tend to have relatively constant evaporation rates throughout the year. Alternatively, Adirondack lake water enrichment could reflect the complex hydrologic drivers of lake water balance. The sampled lakes were selected to represent a wide range of depositional settings (lake and watershed size, fluvial inputs and catchment relief) present in the Adirondacks and therefore basin water balance is likely to vary across the sampled sites, however we are unable to test this fully with the available hydrologic data. While we acknowledge these limitations, the first-order comparison with lake/catchment area ratios suggests that lake water enrichment may instead be driven by the catchment-scale climatic factors listed above (relative humidity, etc), which would theoretically also affect plant source water and, as a result, plant wax δ^2H.

We test the potential link between lake water ^{18}O-enrichment and leaf wax ^2H fractionation by analyzing the relationship between $\varepsilon_{lw\text{-}MAP}$ and ε_{app} in sediments (Fig. EA4). We restricted this analysis to include only the uppermost sample (1.0 to 1.5 cm depth) from each sediment core to reduce the temporal integration represented. The relationships between $\varepsilon_{lw\text{-}MAP}$ and both $\varepsilon_{C29\text{-}MAP}$ and $\varepsilon_{C28\text{-}MAP}$ were not significant (p-values were 0.4 and 0.3, respectively), indicating that sedimentary δ^2H_{wax} is insensitive to the drivers of lake water enrichment, whether those drivers are climatic or related to lake water balance. If lake water enrichment in this study is in fact driven by basin-scale climatic factors, then the corresponding lack of sensitivity of sedimentary δ^2H_{wax} is consistent with observations from other forested biomes (Polissar and Freeman, 2010). This may be because in forested biomes, soil water evaporation (and resulting xylem water ^2H-enrichment) is minimized by tree canopies and groundcover

vegetation structures (e.g., Freimuth et al., 2017). By contrast, in more open ecosystem structures such as grasslands and shrublands local evaporative effects on lake water are also expressed in sedimentary δ^2H_{wax} and this is reflected in significant positive ε_{app}-$\varepsilon_{lw\text{-}MAP}$ slopes (Polissar and Freeman, 2010; Douglas et al., 2012; Fig. EA4).

It remains unclear which specific basin-scale factors (catchment vegetation, local aridity or other unconstrained factors) ultimately control the range of *n*-alkyl lipid distributions and δ^2H observed across the 12 lakes. Basin-scale vegetation differences had an apparently stronger effect on *n*-alkanoic acids, as the abundance and δ^2H of *n*-alkanoic acids varied more widely than *n*-alkanes (Fig. 6 and 7). In addition, there was a greater range of δ^2H_{wax} among lakes for *n*-C_{28} alkanoic acids (35‰) than *n*-C_{29} alkanes (22‰). Together, this suggests greater sensitivity of *n*-alkanoic acid δ^2H to localized basin-scale factors. If this is the case, then *n*-alkanes may more faithfully record regional signals such as δ^2H_p. We explore the regional variability of sedimentary δ^2H_{wax} further in the next section.

4.2. Regional-scale drivers of sedimentary n-alkyl lipid composition

Here, we consider the potential influence of regional climate factors and lipid transport processes on sedimentary δ^2H_{wax} variation. The lakes sampled in this study were selected to maximize basin-scale differences (in forest composition, lake and catchment size and structure) and minimize regional-scale climatic differences by sampling over a relatively small area and elevation range. The OIPC-modeled δ^2H_{MAP} was therefore similar (-76 to -72‰) across the 12 sampled lakes (Bowen and Revenaugh, 2003; Bowen, 2017; Bowen et al., 2005). As a first-order approximation of regional differences in plant source water, OIPC-modeled δ^2H_{MAP} can explain ~34-45% of the variation in sedimentary *n*-C_{27}, *n*-C_{29} and *n*-C_{31} alkane δ^2H at 1 cm core depth (R^2 = 0.42, 0.45, 0.34; p = 0.02, 0.02, 0.05, respectively). While this is an approximation and cannot explain the majority of *n*-alkane δ^2H variation alone, this relationship suggests that sedimentary long-chain *n*-alkane δ^2H is sensitive even to modest regional precipitation signals despite

the considerable basin-scale differences among sites (Table 1). By contrast, OIPC-modeled δ^2H_{MAP} was not significantly correlated with sedimentary *n*-C_{28} or *n*-C_{30} alkanoic acid δ^2H. This reinforces the fidelity of *n*-alkane δ^2H to regional-scale factors and suggests that *n*-alkanoic acids may be more sensitive to basin-scale factors.

Most isoscape models explain the majority of spatial variation in precipitation isotopes as a function of independent variables (including latitude, elevation, mean annual temperature and precipitation amount) that are correlated with precipitation isotope fractionation (Bowen, 2010). Of these variables, latitude can explain ~30-40% of the variation in sedimentary *n*-C_{29} and *n*-C_{31} alkane δ^2H at 1 cm core depth (R^2 = 0.4, 0.3; p = 0.02, 0.04, respectively), possibly reflecting the latitudinal gradient in precipitation (increasing toward the southwest) across the Adirondacks (Ito et al., 2002). This is demonstrated by Wolf and Quiver lakes, which are located at lower latitudes than all other sites (Fig. 1) and had the highest OIPC-modeled δ^2H_{MAP} values (-73‰ and -72‰) and among the highest *n*-alkane δ^2H_{wax} values (Table 1; Fig. 7). Quiver lake also has considerably greater annual precipitation than other sites (Table 1). In addition, *n*-C_{31} alkane δ^2H was correlated with mean annual temperature (R^2 = 0.48; p = 0.01). Elevation was not correlated with sedimentary $^2H_{wax}$, as expected given that the 12 sampled sites were selected to minimize elevation effects on δ^2H_p and therefore δ^2H_{wax}. By contrast, neither latitude or elevation were significantly correlated with *n*-C_{28} or *n*-C_{30} alkanoic acid. This further supports the above evidence suggesting that sedimentary *n*-alkanoic acids are more sensitive to basin-scale factors such as catchment forest composition (see Section 4.1), or that they reflect different source organisms from *n*-alkanes (see Section 4.3).

Relatively invariant long-chain *n*-alkane concentrations across all lakes (Fig. 6), despite the wide range in catchment vegetation mix (Fig. 2) suggests regional-scale integration of long-chain *n*-alkanes. By contrast, *n*-alkanoic acid concentrations vary widely among lakes, suggesting greater sensitivity to basin-scale factors or heterogenous sources. If this contrasting local vs. regional sensitivity for *n*-alkanoic acids and *n*-alkanes is robust, then measuring δ^2H_{wax} from both compounds may have potential to yield

additional environmental information. The δ^2H offset between *n*-C_{29} alkane and the biosynthetic precursor *n*-C_{30} alkanoic acid ($\varepsilon_{C29\text{-}C30}$) varied widely (from -8 to -58‰) among lakes and affords an opportunity to investigate the underlying drivers of this feature.

4.3. Do n-alkanes and n-alkanoic acids record the same water signal?

In Adirondack lake sediments, *n*-alkanoic acid δ^2H values were more positive than *n*-alkane δ^2H, as expected based on prior observations on trees in temperate forested settings (Chikaraishi and Naraoka, 2007; Hou et al., 2007; Freimuth et al., 2017). It was unexpected, however, to find that the magnitude of the δ^2H offset between corresponding *n*-alkanes and their biosynthetic precursor *n*-alkanoic acids ($\varepsilon_{C29\text{-}C30}$ and $\varepsilon_{C27\text{-}C28}$) ranged so widely among lakes (Fig. 8). For instance, a prior study tracked seasonal changes in $\varepsilon_{C29\text{-}C30}$ in five DA tree species occupying the same temperate forest and found that once spring leaves mature, $\varepsilon_{C29\text{-}C30}$ values of approximately -20‰ are established in all species (Freimuth et al., 2017). If sedimentary long-chain *n*-alkanes and *n*-alkanoic acids in the Adirondacks are both derived mainly from tree sources, we would therefore expect sedimentary $\varepsilon_{C29\text{-}C30}$ values of approximately -20‰, but instead values ranged from -8 to -58‰ (Fig. 8). One explanation for this could be that sedimentary *n*-alkanes and *n*-alkanoic acids are sourced from different organisms. While long-chain *n*-alkanes and *n*-alkanoic acids are generally derived from terrestrial higher plants (Ficken et al., 2000; Bush and McInerney, 2013), *n*-C_{28} and *n*-C_{30} alkanoic acids in lake sediments can also reflect aquatic source organisms (whether aquatic plants or microalgae) that access lake water (Polissar et al., 2014; van Bree et al., 2018). Recent studies including multiple *n*-alkyl lipids have also found evidence for variable temporal and spatial sourcing between functionalized lipids and *n*-alkanes (e.g., more rapid and local sourcing of *n*-alkanoic acids compared to *n*-alkanes; Hemingway et al., 2016).

We explored sourcing differences between *n*-alkanoic acids and *n*-alkanes in the context of bulk sediment organic matter. We observed a strong positive correlation between bulk sediment C/N and $\varepsilon_{C29\text{-}C30}$ (R^2 =

0.7, $p < 0.0001$) in Adirondack lakes, wherein $\varepsilon_{C29\text{-}C30}$ was largest in lakes with low C/N and thus greater aquatic organic matter input (excluding one C/N outlier from Little Green; Fig. 8). By contrast, the relationship between $\varepsilon_{C27\text{-}C28}$ and C/N was far weaker ($R^2 = 0.17$, $p = 0.02$), indicating that this relationship is specific to the longer chain-lengths. Emergent and submerged aquatic plants tend to produce higher concentrations of total *n*-alkanoic acids (*n*-$C_{14\text{-}34}$) than total *n*-alkanes (*n*-$C_{19\text{-}35}$), and while submerged aquatic plants generally have *n*-alkanoic acid C_{max} between $C_{20\text{-}24}$, emergent aquatics tend to have higher and more variable C_{max}, ranging from $C_{22\text{-}32}$ (Ficken et al., 2000). C/N ratios are generally ≥ 20 in terrestrial vascular land plants, range widely in emergent and submerged aquatic plants (from approximately 10 to >40), and are generally lowest (approximately 4-10) in lacustrine algae (Cloern et al., 2002; Meyers, 2003). The lakes in this study had mean C/N ratios between 12 and 16 (Table 1), suggesting mixed organic matter sourcing from algae and aquatic and terrestrial plants. It is therefore possible that the relationship between $\varepsilon_{C29\text{-}C30}$ and C/N is linked to lipids sourced from emergent or submerged aquatic plants and their use of lake water. Long-chain *n*-alkanoic acids can be sourced from lacustrine microalgae (Volkman et al., 1998; Ladd et al., 2018; van Bree et al., 2018), which could potentially account for lower (aquatic-derived) C/N sediments having the largest $\varepsilon_{C29\text{-}C30}$ values, reflecting contrasting (terrestrial or aquatic) water sources for *n*-alkanes and *n*-alkanoic acids, respectively.

The abundance ratios of total long-chain *n*-alkanes to *n*-alkanoic acids suggested EG plants as a potentially important source for long-chain *n*-alkanoic acids in sediments as well (Section 4.1.1). We note, however, that EG plants sampled in this study are distinguished by having a higher abundance ratio of *n*-C_{30} acid relative to *n*-C_{28} acid on average (3.6), whereas the opposite is true for both DA plants (0.3) and sediments (which ranged from 0.34 to 0.65; Fig. 6). The abundance ratio of *n*-C_{30} to *n*-C_{28} acid was positively correlated with both C/N and $\varepsilon_{C29\text{-}C30}$ values ($R^2 = 0.46$ and 0.45, respectively, $p < 0.0001$). This supports an aquatic source for *n*-alkanoic acids because in sediments where terrestrial organic matter contributions are minimal (lowest C/N ratios) and an EG plant source of *n*-alkanoic acids in particular is

unlikely (based on low *n*-C_{30} to *n*-C_{28} acid ratios), $\varepsilon_{C29\text{-}C30}$ values were also largest, perhaps reflecting contrasting source water in aquatic-derived *n*-alkanoic acids and terrestrial plant-derived *n*-alkanes.

4.4. ε_{app} in the Adirondacks compared with other biomes

Regional ε_{app} estimates for the Adirondacks (based on OIPC-modeled δ^2H_{MAP} at each site) were -123 ± 6‰ (n = 36) for $\varepsilon_{C29\text{-}MAP}$ and -97 ± 10‰ (n = 34) for $\varepsilon_{C28\text{-}MAP}$ (Table 3). Adirondack $\varepsilon_{C29\text{-}MAP}$ values were smaller than $\varepsilon_{C29\text{-}MAP}$ from comparable lake sediments in cool and temperate forested sites (Table EA2; Fig. EA5) in Europe, North America and Asia (-137 to -131‰; Sachse et al., 2004; Polissar and Freeman, 2010; Seki et al., 2010), perhaps due to differences in precipitation seasonality among sites. The mixed (DA/EG) forest composition in the Adirondacks is unlikely to account for smaller ε_{app} in the Adirondacks because there was no significant difference in δ^2H_{xw} or δ^2H_{wax} between EG and DA plants in this study (Section 3.2.2 and 3.4) or others (Chikaraishi and Naraoka, 2003; Sachse et al., 2004; Gao et al., 2014). We also compared available lake surface sediment ε_{app} data by biome (based on the BIOME4 model of Kaplan et al. (2003), see Table EA2), and found that $\varepsilon_{C29\text{-}MAP}$ values overlap in all biomes represented. Mean $\varepsilon_{C29\text{-}MAP}$ values ranged from -130‰ in temperate forests and -129‰ in Alaskan tundra to -125‰ in tropical forest, grass and shrublands, -120‰ in cool/cold forests and -118‰ in temperate grass and shrublands (Table EA2; Fig. EA5). By comparison, mean $\varepsilon_{C28\text{-}MAP}$ values were similar for lakes in cool/cold, temperate and tropical settings (both forests and grass or shrublands), ranging from -105 to -95‰, but distinct from the Alaskan tundra (-127‰, Daniels et al., 2017; Table EA2 and Fig. EA5). Two main insights about *n*-alkyl lipids in lake sediments result from this comparison. First, across major climate zones, mean $\varepsilon_{C29\text{-}MAP}$ values are similar (ranging ~10‰), whereas mean $\varepsilon_{C28\text{-}MAP}$ values are more variable (ranging ~30‰). Second, in all major climate zones aside from the Alaskan tundra, ε_{app} values are smaller for *n*-C_{28} alkanoic acids than for *n*-C_{29} alkanes.

Numerous calibration studies have sampled lake surface sediments along gradients in climate and vegetation in order to evaluate their effects on sedimentary δ^2H_{wax}. By contrast, this study aimed to understand the influence of basin-scale effects on sedimentary δ^2H_{wax} by sampling 12 lakes in the same region with minimal differences in climate and vegetation (all catchments were forested, with a range of DA/EG abundance ratios; Fig. 2). Across the Adirondack sites, estimated δ^2H_{MAP} ranged by less than 10‰, while δ^2H_{wax} ranged by 22 to 35‰ for *n*-alkanes and *n*-alkanoic acids. Two other studies have taken a comparable approach, sampling 24 lakes in the Alaskan tundra (Daniels et al., 2017) and 20 lakes in the Central American and Mexican tropics (Douglas et al., 2012). In the Alaskan tundra, δ^2H_p differences among sites are likely minimal (the sampled lakes are within a ~500 km^2 area), while δ^2H_{wax} ranged by up to 37‰ for *n*-alkanoic acids and 32‰ for *n*-alkanes (Daniels et al., 2017). In the tropics, the estimated total range in δ^2H_p was 25‰, while δ^2H_{wax} ranged by 60‰ for *n*-alkanoic acids and 56‰ for *n*-alkanes (Douglas et al., 2012). The δ^2H_{wax} variability in the tropics was nearly twice as large as in the Adirondacks or Alaskan tundra. The variability in δ^2H_{wax} in the tropics is largely explained by the aridity index (the ratio of mean annual precipitation to potential evapotranspiration (MAP/PET); Douglas et al., 2012), which is not a significant control in the Adirondacks (see Section 4.1.2) or the Alaskan tundra, where basin-scale vegetation effects may be a controlling factor (Daniels et al., 2017). Together these studies provide preliminary estimates of the maximum expected basin-to-basin variability in lake sediment δ^2H_{wax}, which is approximately 20 to 30‰ due to basin-scale vegetation effects in regions with high MAP/PET, or approximately 50 to 60‰ due to basin-scale aridity effects in regions with low MAP/PET.

These three studies also measured δ^2H_{wax} on both *n*-alkanes and *n*-alkanoic acids in the same samples and therefore offer an opportunity to compare $\varepsilon_{C29\text{-}C30}$ across biomes. Mean $\varepsilon_{C29\text{-}C30}$ was distinct among climates, with smaller values in the tropics (-7 ± 10‰, n = 11; Douglas et al., 2012), intermediate values in the Alaskan tundra (-17 ± 10‰, n = 16; Daniels et al., 2017) and highest values in this study (-35 ±

12‰, n = 12; ANOVA, $R^2 = 0.55$, $p < 0.0001$). The trends in lake sediments reflect observations on *n*-alkanes and *n*-alkanoic acids in plants, where tropical forests had a mean $\varepsilon_{C29\text{-}C30}$ of only -3 ± 17‰ (n = 64 individuals, 16 species; Feakins et al., 2016) compared with $\varepsilon_{C29\text{-}C30}$ of -20 to -30‰ for temperate forests (Chikaraishi and Naraoka, 2007; Hou et al., 2007; Freimuth et al., 2017). It is unclear what controls the differences in $\varepsilon_{C29\text{-}C30}$ between temperate and tropical regions, but future studies including both *n*-alkanes and *n*-alkanoic acids in plants and sediments could test climatic and vegetation effects with potential implications for reconstructing such effects in the past using paired δ^2H_{wax} on both compounds.

5. Conclusions

This study measured the δ^2H_{wax} signal in lake surface sediments throughout a cool mixed forest biome, the Adirondack Mountains, to determine the degree to which catchment-specific factors affect the fidelity of plant waxes as tracers of water isotopes. Based on plant water and surface water isotope measurements, plant source waters reflect annually-integrated precipitation values and do not vary systematically among sites. If sedimentary plant wax primarily reflects plant source water, then we would also expect δ^2H_{wax} to be similar among the 12 lakes sampled. However, sedimentary δ^2H_{wax} values ranged by up to 22‰ for *n*-C_{29} alkane and 35‰ for *n*-C_{28} alkanoic acid. The abundance of long-chain *n*-alkanes in sediments was remarkably consistent among lakes, despite the range of forest assemblages and the considerable differences in *n*-alkane production between DA and EG trees. By contrast, the abundance of long-chain *n*-alkanoic acids in sediments varied by an order of magnitude among different lakes. The extent of evergreen vegetation in lake shorelines was correlated with the abundance ratio of long-chain *n*-alkanes relative to *n*-alkanoic acids, which may indicate sourcing of *n*-alkanoic acids in part from EG trees. These data suggest that sedimentary *n*-alkanoic acids may be more sensitive than *n*-alkanes to basin-scale factors such as catchment vegetation cover.

The δ^2H offset between *n*-C_{29} alkane and the biosynthetic precursor *n*-C_{30} alkanoic acid ($\varepsilon_{C29\text{-}C30}$) ranged from -8 to -58‰ among sites and was strongly correlated with sediment C/N ratios. This relationship supports an aquatic source for long-chain *n*-alkanoic acids. We found larger ε_{app} for *n*-alkanes (-123‰) than for *n*-alkanoic acids (-97‰). In the absence of a gradient in δ^2H_p over the sampled region, we observed higher site-to-site variability in long-chain *n*-alkanoic acid abundance and δ^2H values compared to long-chain *n*-alkanes. The evidence for basin-scale effects on sedimentary *n*-alkanoic acids suggests that they are primarily sourced from within a lake catchment rather than mixed at a regional scale. By contrast, *n*-alkanes were relatively insensitive to basin-scale factors such as forest composition, which reinforces their utility as tracers for regional-scale δ^2H_p from lake sediments in similar settings.

Acknowledgements:

We thank the New York State Department of Environmental Conservation, especially Jonathan DeSantis and Barbara Lucas-Wilson, for sampling permits (TRP #2349/10310). Daphne Taylor and Natasha Karniski at the SUNY-ESF Newcomb campus provided access to Wolf Pond and the Adirondack Mountain Club granted access to Heart Lake. Thanks go to Elliot Boyd, Helen Eifert and Thomas Faraday for field sampling assistance, and to Andrew Diefendorf for designing and building refrigerated core storage and an essential core splitter. Paul McKenzie provided temporary core storage and Kelly Grogan assisted with sample preparation. This research was supported by the US National Science Foundation (EAR-1229114 to AFD, EAR-1636740 to AFD and TVL and EAR-1636744 to AKS) and by a University of Cincinnati Research Council award to EJF.

REFERENCES

Aichner B., Herzschuh U. and Wilkes H. (2010) Influence of aquatic macrophytes on the stable carbon isotopic signatures of sedimentary organic matter in lakes on the Tibetan Plateau. *Org. Geochem.* **41**, 706-718.

Bai H., Peng L., Li Z., Liu X., Song C. and Mu L. (2014) Compound-specific hydrogen isotope composition of *n*-alkanes in combustion residuals of fossil fuels. *Atmos. Environ.* **97**, 28–34.

Bi X., Sheng G., Liu X., Li C. and Fu J. (2005) Molecular and carbon and hydrogen isotopic composition of *n*-alkanes in plant leaf waxes. *Org. Geochem.* **36**, 1405-1417.

Binford M.W. (1990) Calculation and uncertainty analysis of ^{210}Pb dates for PIRLA project lake sediment cores. *J. Paleolimn.* **3**, 253-267.

Binford M.W., Kahl J.S. and Norton S.A. (1993) Interpretation of ^{210}Pb profiles and verification of the CRS dating model in PIRLA project lake sediment cores. *J. Paleolimn.* **9**, 275-296.

Bird B.W., Polisar P.J., Lei Y., Thompson L.G., Yao T., Finney B.P., Bain D.J., Pompeani D.P. and Steinman B.A. (2014) A Tibetan lake sediment record of Holocene Indian summer monsoon variability. *Earth Planet. Sci. Lett.* **399**, 92-102.

Bowen G.J. (2010) Isoscapes: spatial pattern in isotopic biogeochemistry. *Annu. Rev. Earth Planet. Sci.* **38**, 161-187.

Bowen G.J. (2017) The Online Isotopes in Precipitation Calculator, version 3.1. http://www.waterisotopes.org.

Bowen G.J. and Revenaugh J. (2003) Interpolating the isotopic composition of modern meteoric precipitation. *Water Resour. Res.* **39**, 1299.

Bowen G.J., Wassenaar L.I. and Hobson K.A. (2005) Global application of stable hydrogen and oxygen isotopes to wildlife forensics. *Oecologia* **143**, 337-348.

Brodribb T.J., Pittermann J. and Coomes D.A. (2012) Elegance versus speed: examining the competition between conifer and angiosperm trees. *Int. J. Plant Sci.* **173**, 673-694.

Brooks J.R., Gibson J.J., Birks S.J., Weber M.H., Rodecap K.D. and Stoddard J.L. (2014) Stable isotope estimates of evaporation: inflow and water residence time for lakes across the United States as a tool for national lake water quality assessments. *Limnol. Oceanogr.* **59**, 2150-2165.

Bush R.T. and McInerney F.A. (2013) Leaf wax *n*-alkane distributions in and across modern plants: Implications for paleoecology and chemotaxonomy. *Geochim. Cosmochim. Acta* **117**, 161-179.

Carmichael M.J., Inglis G.N., Badger M.P., Naafs B.D.A., Behrooz L., Remmelzwaal S., Monteiro F.M., Rohrssen M., Farnsworth A., Buss H.L. and Dickson A.J. (2017) Hydrological and associated biogeochemical consequences of rapid global warming during the Paleocene-Eocene Thermal Maximum. *Glob. Planet. Change* **157**, 114-138.

Castañeda I.S. and Schouten S. (2011) A review of molecular organic proxies for examining modern and ancient lacustrine environments. *Quat. Sci. Rev.* **30**, 2851-2891.

Charles D.F., Binford M.W., Furlong E.T., Hites R.A., Mitchell M.J., Norton S.A., Oldfield F., Paterson M.J., Smol J.P. and Uutala A.J. (1990) Paleoecological investigation of recent lake acidification in the Adirondack Mountains, NY. *J. Paleolimn.* **3**, 195-241.

Chikaraishi Y. and Naraoka H. (2003) Compound-specific δ^2H-δ^{13}C analyses of *n*-alkanes extracted from terrestrial and aquatic plants. *Phytochemistry* **63**, 361-371.

Chikaraishi Y. and Naraoka H. (2007) δ^{13}C and δ^2H relationships among three *n*-alkyl compound classes (*n*-alkanoic acid, *n*-alkane and *n*-alkanol) of terrestrial higher plants. *Org. Geochem.* **38**, 198-215.

Clark I.D. and Fritz P. (1997) *Environmental Isotopes in Hydrogeology*. Lewis Publishers, New York.

Cloern J.E., Canuel E.A. and Harris D. (2002) Stable carbon and nitrogen isotope composition of aquatic and terrestrial plants of the San Francisco Bay estuarine system. *Limnol. Oceanogr.* **47**, 713-729.

Coplen T.B. (1988) Normalization of oxygen and hydrogen isotope data. *Chem. Geol.* **72**, 293-297.

Coplen T.B. and Huang R. (2000) Stable hydrogen and oxygen isotope ratios for selected sites of the National Oceanic and Atmospheric Administration's Atmospheric Integrated Research Monitoring Network (AIRMoN). *US Geological Survey Open-File Report 00-279*: Reston, 54.

Coplen T.B., Brand W.A., Gehre M., Gröning M., Meijer H.A.J., Toman B. and Verkouteren R.M. (2006) New guidelines for $\delta^{13}C$ measurements. *Anal. Chem.* **78**, 2439-2441.

Cormier M.A., Werner R.A., Sauer P.E., Gröcke D.R., Leuenberger M.C., Wieloch T., Schleucher J. and Kahmen A. (2018) ^{2}H-fractionations during the biosynthesis of carbohydrates and lipids imprint a metabolic signal on the $\delta^{2}H$ values of plant organic compounds. *New Phytol.* **218**, 479-491.

Daniels W.C., Russell J.M., Giblin A.E., Welker J.M., Klein E.S. and Huang Y. (2017) Hydrogen isotope fractionation in leaf waxes in the Alaskan Arctic tundra. *Geochim. Cosmochim. Acta* **213**, 216-236.

Dansgaard W. (1964) Stable isotopes in precipitation. *Tellus* **16**, 436-468.

Diefendorf A.F., Patterson W.P., Holmden C. and Mullins H.T. (2008) Carbon isotopes of marl and lake sediment organic matter reflect terrestrial landscape change during the late Glacial and early Holocene (16,800 to 5,540 cal yr BP): a multiproxy study of lacustrine sediments at Lough Inchiquin, western Ireland. *J. Paleolimn.* **39**, 101-115.

Diefendorf A.F., Freeman K.H., Wing S.L. and Graham H.V. (2011) Production of *n*-alkyl lipids in living plants and implications for the geologic past. *Geochim. Cosmochim. Acta* **75**, 7472-7485.

Diefendorf A.F., Leslie A.B. and Wing S.L. (2015) Leaf wax composition and carbon isotopes vary among major conifer groups. *Geochim. Cosmochim. Acta* **170**, 145-156.

Diefendorf A.F. and Freimuth E.J. (2017) Extracting the most from terrestrial plant-derived *n*-alkyl lipids and their carbon isotopes from the sedimentary record: A review. *Org. Geochem.* **103**, 1-21.

Douglas P.M.J., Pagani M., Brenner M., Hodell D.A. and Curtis J.H. (2012) Aridity and vegetation composition are important determinants of leaf-wax $\delta^{2}H$ values in southeastern Mexico and Central America. *Geochim. Cosmochim. Acta* **97**, 24-45.

Driscoll C., Poster K., Kretser W. and Raynal D. (1995) Long-term trends in the chemistry of precipitation and lake water in the Adirondack region of New York, USA. *Water Air Soil Pollut.* **85**, 583-588.

Driscoll C.T. and Newton R.M. (1985) Chemical characteristics of Adirondack lakes. *Environ. Sci. Technol.* **19**, 1018-1024.

Driscoll C.T., Newton R.M., Gubala C.P., Baker J.P. and Christensen S.W. (1991) Adirondack Mountains. In *Acidic Deposition and Aquatic Ecosystems* (eds. D.F. Charles and S. Christie). Springer, New York, 133-202.

Eley Y., Dawson L., Black S., Andrews J. and Pedentchouk N. (2014) Understanding $^{2}H/^{1}H$ systematics of leaf wax *n*-alkanes in coastal plants at Stiffkey saltmarsh, Norfolk, UK. *Geochim. Cosmochim. Acta* **128**, 13-28.

Evaristo J. and McDonnell J.J. (2017) Prevalence and magnitude of groundwater use by vegetation: a global stable isotope meta-analysis. *Sci. Rep.* **7**, 44110.

Evaristo J., McDonnell J.J. and Clemens J. (2017) Plant source water apportionment using stable isotopes: A comparison of simple linear, two-compartment mixing model approaches. *Hydrol. Process.* **31**, 3750-3758.

Feakins S.J., Eglinton T.I., deMenocal P.B. (2007) A comparison of biomarker records of northeast African vegetation from lacustrine and marine sediments (ca. 3.40 Ma). *Org. Geochem.* **38**, 1607-1624.

Feakins S.J. and Sessions A.L. (2010) Controls on the D/H ratios of plant leaf waxes from an arid ecosystem. *Geochim. Cosmochim. Acta* **74**, 2128-2141.

Feakins S.J., Kirby M.E., Cheetham M.I., Ibarra Y. and Zimmerman S.R.H. (2014) Fluctuation in leaf wax D/H ratio from a southern California lake records significant variability in isotopes in precipitation during the late Holocene. *Org. Geochem.* **66**, 48-59.

Feakins S.J., Bentley L.P., Salinas N., Shenkin A., Blonder B., Goldsmith G.R., Ponton C., Arvin L.J., Wu M.S., Peters T. and West A.J. (2016) Plant leaf wax biomarkers capture gradients in hydrogen isotopes of precipitation from the Andes and Amazon. *Geochim. Cosmochim. Acta* **182**, 155-172.

Feakins S.J., Wu M.S., Ponton C., Galy V. and West A.J. (2018) Dual isotope evidence for sedimentary integration of plant wax biomarkers across an Andes-Amazon elevation transect. *Geochim. Cosmochim. Acta* **242**, 64-81.

Ficken K.J., Li B., Swain D.L. and Eglinton G. (2000) An *n*-alkane proxy for the sedimentary input of submerged/floating freshwater aquatic macrophytes. *Org. Geochem.* **31**, 745-749.

Freeman K.H. and Pancost R.D. (2014) Biomarkers for Terrestrial Plants and Climate. In *Treatise on Geochemistry (Second Edition)* (ed. H.D. Holland and K.K. Turekian). Elsevier, Oxford, 395-416.

Freimuth E.J., Diefendorf A.F. and Lowell T.V. (2017) Hydrogen isotopes of *n*-alkanes and *n*-alkanoic acids as tracers of precipitation in a temperate forest and implications for paleorecords. *Geochim. Cosmochim. Acta* **206**, 166-183.

Freimuth E.J., Diefendorf A.F., Lowell T.V. and Wiles G.C. (2019) Sedimentary n-alkanes and n-alkanoic acids in a temperate bog are biased toward woody plants. *Org. Geochem.* **128**, 94-107.

Gao L., Edwards E.J., Zeng Y. and Huang Y. (2014) Major evolutionary trends in hydrogen isotope fractionation of vascular plant leaf waxes. *PLoS ONE* **9**, e112610.

Garcin Y., Schwab V.F., Gleixner G., Kahmen A., Todou G., Séné O., Onana J.-M., Achoundong G. and Sachse D. (2012) Hydrogen isotope ratios of lacustrine sedimentary *n*-alkanes as proxies of tropical African hydrology: insights from a calibration transect across Cameroon. *Geochim. Cosmochim. Acta* **79**, 106-126.

Gat J.R. (1995) Stable isotopes of fresh and saline lakes. In *The Physics and Chemistry of Lakes* (ed. A. Lerman, D.M. Imboden, and J.R. Gat). Springer-Verlag, New York, 139-164.

Gibson J.J. and Edwards T.W.D. (2002) Regional water balance trends and evaporation-transpiration partitioning from a stable isotope survey of lakes in northern Canada. *Global Biogeochem. Cy.* **16**, 10-1.

Gibson J.J., Birks S.J. and Edwards T.W.D. (2008) Global prediction of δ_A and δ^2H-$\delta^{18}O$ evaporation slopes for lakes and soil water accounting for seasonality. *Global Biogeochem. Cy.* **22**, GB2031.

Giri S.J., Diefendorf A.F. and Lowell T.V. (2015) Origin and sedimentary fate of plant-derived terpenoids in a small river catchment and implications for terpenoids as quantitative paleovegetation proxies. *Org. Geochem.* **82**, 22-32.

Gray A.B., Pasternack G.B. and Watson E.B. (2010) Hydrogen peroxide treatment effects on the particle size distribution of alluvial and marsh sediments. *The Holocene* **20**, 293-301.

Heiri O., Lotter A.F. and Lemcke G. (2001) Loss on ignition as a method for estimating organic and carbonate content in sediments: reproducibility and comparability of results. *J. Paleolimn.* **25**, 101-110.

Hemingway J.D., Schefuß E., Dinga B.J., Pryer H. and Galy V.V. (2016) Multiple plant-wax compounds record differential sources and ecosystem structure in large river catchments. *Geochim. Cosmochim. Acta* **184**, 20-40.

Homer C., Dewitz J., Yang L., Jin S., Danielson P., Xian G., Coulston J., Herold N., Wickham J. and Megown K. (2015) Completion of the 2011 National Land Cover Database for the conterminous United States–representing a decade of land cover change information. *Photogramm. Eng. Remote Sensing* **81**, 345-354.

Hou J.Z., D'Andrea W.J., MacDonald D. and Huang Y.S. (2007) Hydrogen isotopic variability in leaf waxes among terrestrial and aquatic plants around Blood Pond, Massachusetts (USA). *Org. Geochem.* **38**, 977-984.

IAEA/WMO (2018). Global Network of Isotopes in Precipitation. The GNIP Database. Accessible at: https://nucleus.iaea.org/wiser.

Ito M., Mitchell M.J. and Driscoll C.T. (2002) Spatial patterns of precipitation quantity and chemistry and air temperature in the Adirondack region of New York. *Atmos. Environ.* **36**, 1051-1062.

Kahmen A., Hoffmann B., Schefuß E., Arndt S.K., Cernusak L.A., West J.B. and Sachse D. (2013a) Leaf water deuterium enrichment shapes leaf wax *n*-alkane δ^2H values of angiosperm plants II: Observational evidence and global implications. *Geochim. Cosmochim. Acta* **111**, 50-63.

Kahmen A., Schefuß E. and Sachse D. (2013b) Leaf water deuterium enrichment shapes leaf wax *n*-alkane δ^2H values of angiosperm plants I: Experimental evidence and mechanistic insights. *Geochim. Cosmochim. Acta* **111**, 39-49.

Kaplan J.O., Bigelow N.H., Prentice I.C., Harrison S.P., Bartlein P.J., Christensen T.R., Cramer W., Matveyeva N.V., McGuire A.D., Murray D.F. and Razzhivin V.Y. (2003) Climate change and Arctic ecosystems: 2. Modeling, paleodata-model comparisons, and future projections. *J. Geophys. Res. Atmos.* **108**, D19.

Kendall C. and Coplen T.B. (2001) Distribution of oxygen-18 and deuterium in river waters across the United States. *Hydrol. Process.* **15**, 1363-1393.

Ladd S.N., Nelson D.B., Schubert C.J. and Dubois N. (2018) Lipid compound classes display diverging hydrogen isotope responses in lakes along a nutrient gradient. *Geochim. Cosmochim. Acta* **237**, 103-119.

Liu H. and Liu W. (2016) *n*-Alkane distributions and concentrations in algae, submerged plants and terrestrial plants from the Qinghai-Tibetan Plateau. *Org. Geochem.* **99**, 10-22.

Marzi R., Torkelson B.E. and Olson R.K. (1993) A revised carbon preference index. *Org. Geochem.* **20**, 1303-1306.

McInerney F.A., Helliker B.R. and Freeman K.H. (2011) Hydrogen isotope ratios of leaf wax *n*-alkanes in grasses are insensitive to transpiration. *Geochim. Cosmochim. Acta* **75**, 541-554.

Meyers P.A. (2003) Applications of organic geochemistry to paleolimnological reconstructions: a summary of examples from the Laurentian Great Lakes. *Org. Geochem.* **34**, 261-289.

Meyers P.A. and Ishiwatari R. (1993) Lacustrine organic geochemistry—an overview of indicators of organic matter sources and diagenesis in lake sediments. *Org. Geochem.* **20**, 867-900.

Newberry S.L., Kahmen A., Dennis P. and Grant A. (2015) *n*-Alkane biosynthetic hydrogen isotope fractionation is not constant throughout the growing season in the riparian tree *Salix viminalis*. *Geochim. Cosmochim. Acta* **165**, 75-85.

Niedermeyer E.M., Sessions A.L., Feakins S.J. and Mohtadi M. (2014) Hydroclimate of the western Indo-Pacific Warm Pool during the past 24,000 years. *Proc. Natl. Acad. Sci.* **111**, 9402-9406.

Pancost R.D. and Boot C.S. (2004) The palaeoclimatic utility of terrestrial biomarkers in marine sediments. *Mar. Chem.* **92**, 239-261.

Paul D. and Skrzypek G. (2006) Flushing time and storage effects on the accuracy and precision of carbon and oxygen isotope ratios of sample using the Gasbench II technique. *Rapid Commun. Mass Spectrom.* **20**, 2033-2040.

Pedentchouk N., Sumner W., Tipple B. and Pagani M. (2008) $\delta^{13}C$ and δ^2H compositions of *n*-alkanes from modern angiosperms and conifers: An experimental set up in central Washington State, USA. *Org. Geochem.* **39**, 1066-1071.

Peel M.C., Finlayson B.L. and McMahon T.A. (2007) Updated world map of the Köppen-Geiger climate classification. *Hydrol. Earth Syst. Sci.* **11**, 1633-1644.

Polissar P.J. and D'Andrea W.J. (2014) Uncertainty in paleohydrologic reconstructions from molecular δD values. *Geochim. Cosmochim. Acta* **129**, 146-156.

Polissar P.J., Preefer M. and Liu C. (2014) Fidelity of leaf-wax *n*-alkane and *n*-alkanoic acid D/H ratios in space and time, American Geophysical Union, PP43E-07.

Polissar P.J. and Freeman K.H. (2010) Effects of aridity and vegetation on plant-wax δ^2H in modern lake sediments. *Geochim. Cosmochim. Acta* **74**, 5785-5797.

PRISM Climate Group (2018) Oregon State University, http://prism.oregonstate.edu.

Rach O., Brauer A., Wilkes H. and Sachse D. (2014) Delayed hydrological response to Greenland cooling at the onset of the Younger Dryas in western Europe. *Nat. Geosci.* **7**, 109-112.

Sachse D., Radke J. and Gleixner G. (2004) Hydrogen isotope ratios of recent lacustrine sedimentary *n*-alkanes record modern climate variability. *Geochim. Cosmochim. Acta* **68**, 4877-4889.

Sachse D., Radke J. and Gleixner G. (2006) δ^2H values of individual *n*-alkanes from terrestrial plants along a climatic gradient – Implications for the sedimentary biomarker record. *Org. Geochem.* **37**, 469-483.

Sachse D., Gleixner G., Wilkes H. and Kahmen A. (2010) Leaf wax *n*-alkane δ^2H values of field-grown barley reflect leaf water δ^2H values at the time of leaf formation. *Geochim. Cosmochim. Acta* **74**, 6741-6750.

Sachse D., Billault I., Bowen G.J., Chikaraishi Y., Dawson T.E., Feakins S.J., Freeman K.H., Magill C.R., McInerney F.A., van der Meer M.T.J., Polissar P., Robins R.J., Sachs J.P., Schmidt H.-L., Sessions A.L., White J.W.C., West J.B. and Kahmen A. (2012) Molecular paleohydrology: Interpreting the hydrogen-isotopic composition of lipid biomarkers from photosynthesizing organisms. *Annu. Rev. Earth Planet. Sci.* **40**, 221-249.

Seki O., Nakatsuka T., Shibata H. and Kawamura K. (2010) A compound-specific *n*-alkane $\delta^{13}C$ and δ^2H approach for assessing source and delivery processes of terrestrial organic matter within a forested watershed in northern Japan. *Geochim. Cosmochim. Acta* **74**, 599-613.

Sessions A.L. (2016) Factors controlling the deuterium contents of sedimentary hydrocarbons. *Org. Geochem.* **96**, 43-64.

Stager J.C., Cumming B.F., Laird K.R., Garrigan-Piela A., Pederson N., Wiltse B., Lane C.S., Nester J. and Ruzmaikin A. (2016) A 1600-year diatom record of hydroclimate variability from Wolf Lake, New York. *The Holocene* **27**, 246-257.

Tierney J.E., Russell J.M., Huang Y., Damsté J.S.S., Hopmans E.C. and Cohen A.S. (2008) Northern hemisphere controls on tropical southeast African climate during the past 60,000 years. *Science* **322**, 252-255.

Tipple B.J. and Pagani M. (2013) Environmental control on eastern broadleaf forest species' leaf wax distributions and D/H ratios. *Geochim. Cosmochim. Acta* **111**, 64-77.

Tipple, B.J. and Ehleringer, J.R. (2018) Distinctions in heterotrophic and autotrophic-based metabolism as recorded in the hydrogen and carbon isotope ratios of normal alkanes. *Oecologia*, **187**, 1053-1075.

van Bree L.G.J., Peterse F., van der Meer M.T.J., Middelburg J.J., Negash A.M.D., De Crop W., Cocquyt C., Wieringa J.J., Verschuren D. and Sinninghe Damsté J.S. (2018) Seasonal variability in the abundance and stable carbon-isotopic composition of lipid biomarkers in suspended particulate matter from a stratified equatorial lake (Lake Chala, Kenya/Tanzania) - Implications for the sedimentary record. *Quat. Sci. Rev.* **192**, 208–224.

van Geldern R. and Barth J.A. (2012) Optimization of instrument setup and post-run corrections for oxygen and hydrogen stable isotope measurements of water by isotope ratio infrared spectroscopy (IRIS). *Limnol. Oceanogr. Methods* **10**, 1024-1036.

Volkman J.K., Barrett S.M., Blackburn S.I., Mansour M.P., Sikes E.L., Gelin F. (1998) Microalgal biomarkers: a review of recent research developments. *Org. Geochem.* **29**, 1163-1179.

West A.G., Patrickson S.J. and Ehleringer J.R. (2006) Water extraction times for plant and soil materials used in stable isotope analysis. *Rapid Commun. Mass Spectrom.* **20**, 1317-1321.

Whitehead D.R., Charles D.F., Jackson S.T., Smol J.P. and Engstrom D.R. (1990) The developmental history of Adirondack (NY) lakes. In *Paleolimnology and the Reconstruction of Ancient Environments* (ed. R.B. Davis). Springer, New York, 169-190.

Figure Captions

Figure 1. Elevation map showing the Adirondack Park border (dashed line) and locations of the 12 sampled lakes (circles): 1, Chazy; 2, Debar; 3, East Pine; 4, Heart; 5, Hope; 6, Horseshoe; 7, Little Green; 8, Moose; 9, Quiver; 10, Raquette; 11, Sucker; 12, Wolf. Precipitation isotope data used in this study were from locations (squares) to the north in Ottawa (IAEA/WMO, 2018) and to the southwest in Tompkins County, NY (Coplen and Huang, 2000).

Figure 2. Vegetation assemblages for: A) each lake catchment, and B) 30 m lake shoreline buffers based on the 2011 National Land Cover Database (NLCD). EG, evergreen gymnosperm; DA, deciduous angiosperm. Sites are ordered by increasing shoreline EG coverage.

Figure 3. Relationship between sediment TOC and $\delta^{13}C_{org}$ at 1, 5, and 9 cm depth in each lake core for basins with no fluvial inputs (filled symbols) and with one or more fluvial inputs (open symbols).

Figure 4. The $\delta^{2}H$ and $\delta^{18}O$ composition of regional precipitation collected at the Ottawa GNIP station (light gray points, solid black line) and modeled (monthly) for the Adirondack lake sites (gray squares, gray dashed line). Adirondack waters collected in this study include lakes (blue points, black dashed line), rivers (red squares), snow events (blue stars) and xylem waters (green triangles). The white diamond ($\delta^{2}H$, -75‰; $\delta^{18}O$, -10.8‰) indicates the intercept of the regional evaporation line (REL) with the regional meteoric water line (RMWL). Also shown are the range of OIPC-modeled $\delta^{2}H_{MAP}$ across all 12 sites (light gray bar, -76 to -72‰) and mean $\delta^{2}H_{xw}$ (green dashed line, -76‰).

Figure 5. Distributions of *n*-C_{17} to *n*-C_{35} alkanes and *n*-C_{28} and *n*-C_{30} alkanoic acids from each lake, in µg wax/g TOC. Dark bars represent odd carbon numbered *n*-alkanes. Bars with hatched fill represent *n*-C_{28}

and *n*-C_{30} alkanoic acid. Error bars represent one standard deviation of the mean for three samples (at 1, 5, and 9 cm) from each sediment core.

Figure 6. Mean long-chain *n*-alkanoic acid (brown) and *n*-alkane (blue) concentrations in µg/g TOC for A) surface sediments from 12 Adirondack lakes (n = 3 samples per lake) and B) leaves of common Adirondack DA (n = 13 individuals, 5 species) and EG (n = 14 individuals, 7 species) plants. Error bars represent one standard error of the mean.

Figure 7. The δ^2H composition of *n*-C_{27}, *n*-C_{29} and *n*-C_{31} alkanes (blue symbols) and *n*-C_{28} and *n*-C_{30} alkanoic acids (brown symbols) in the uppermost Adirondack lake sediments (1.0-1.5 cm depth). Compounds with matching symbol shapes indicate paired *n*-alkanes and precursor *n*-alkanoic acids.

Figure 8. Regression between C/N ratios and $\varepsilon_{C29\text{-}C30}$ values (the δ^2H fractionation between *n*-C_{29} alkane and *n*-C_{30} acid) in sediments. The light gray symbol from Little Green at 1 cm depth is excluded from the analysis. Filled symbols indicate lakes with no fluvial inlets. Shaded area around dashed black line indicates the 90% confidence interval. Horizontal gray bar indicates the expected total range of $\varepsilon_{C29\text{-}C30}$ in Adirondack sediments based on prior studies of temperate plants (Chikaraishi and Naraoka, 2007; Hou et al., 2007; Freimuth et al., 2017).

Figure 9. The relationship between shoreline evergreen land cover and the abundance ratio of long-chain (*n*-C_{27} to *n*-C_{35}) alkanes to (*n*-C_{28} and *n*-C_{30}) alkanoic acids in Adirondack lake sediments. Dashed regression line excludes the open points representing sediments from the two dammed sites, Chazy and Raquette.

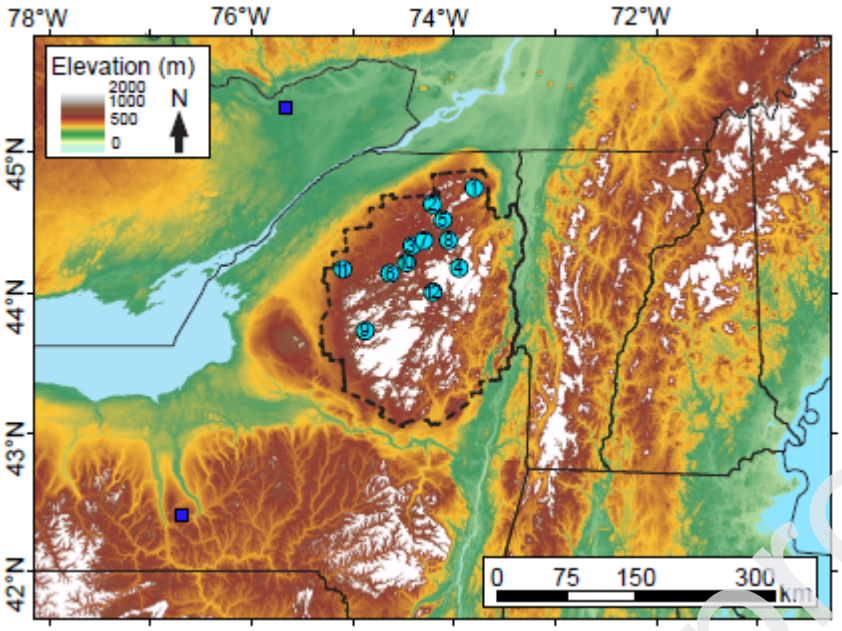

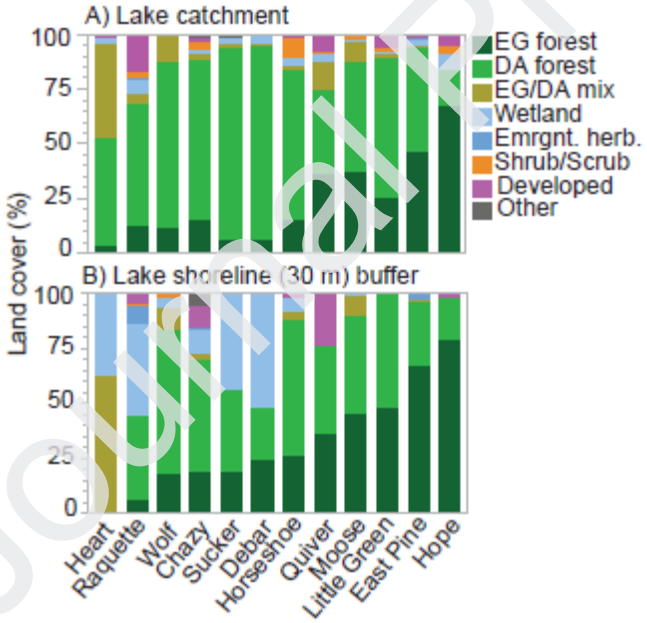

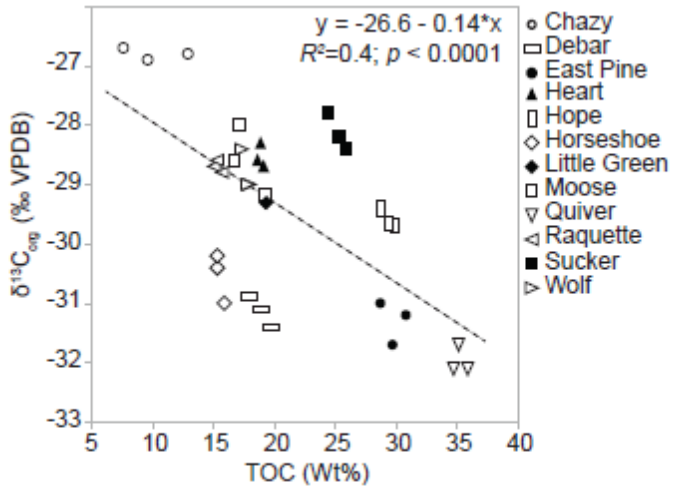

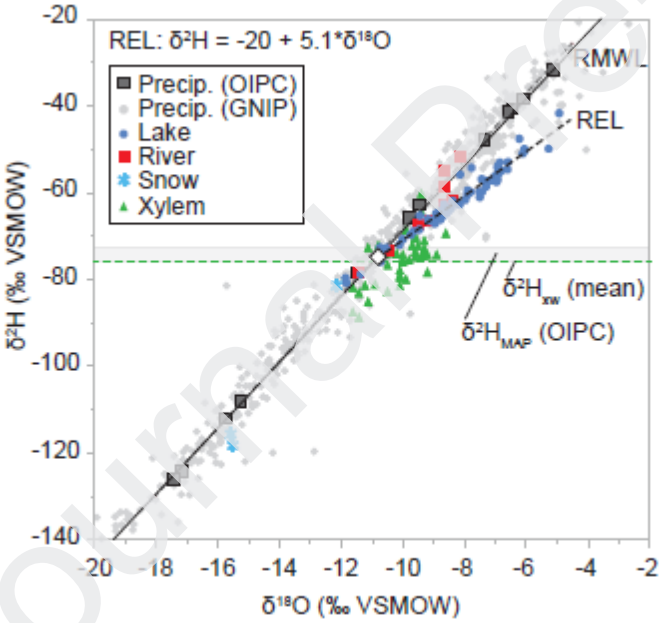

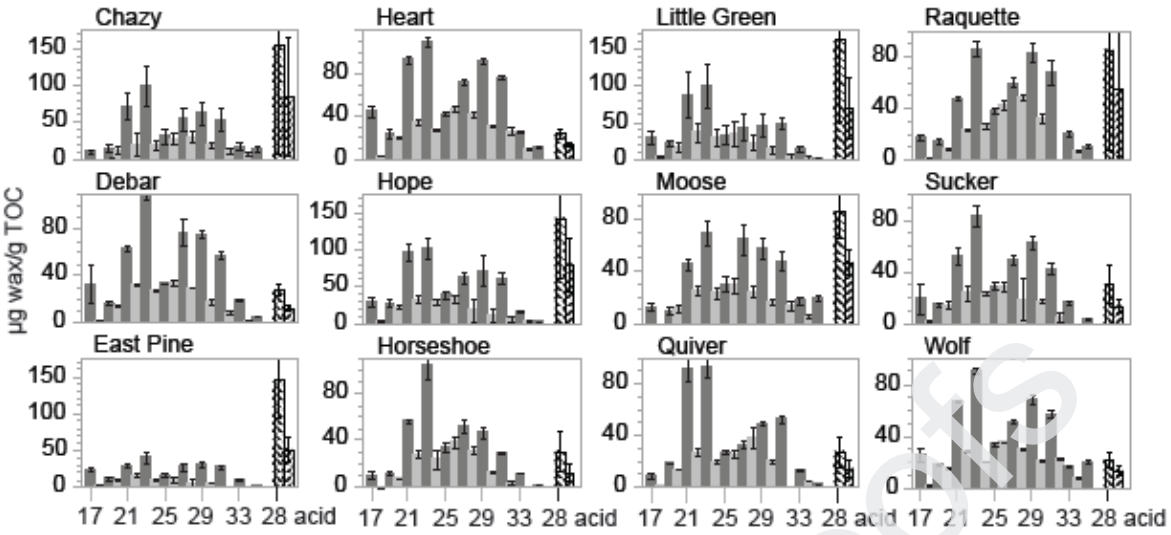

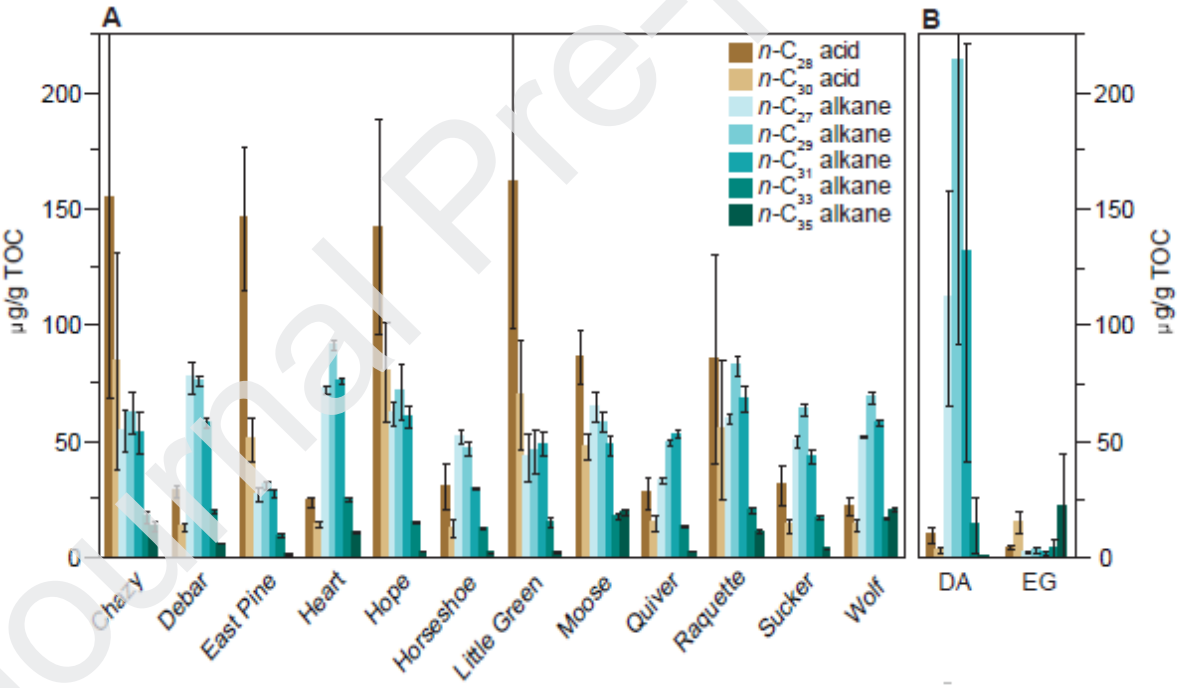

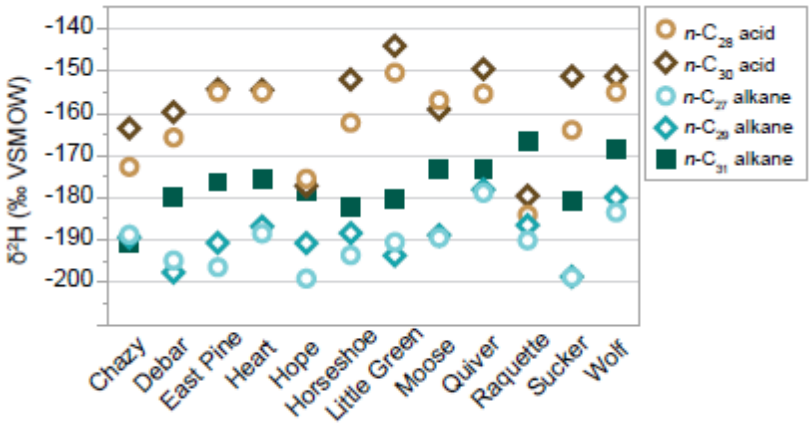

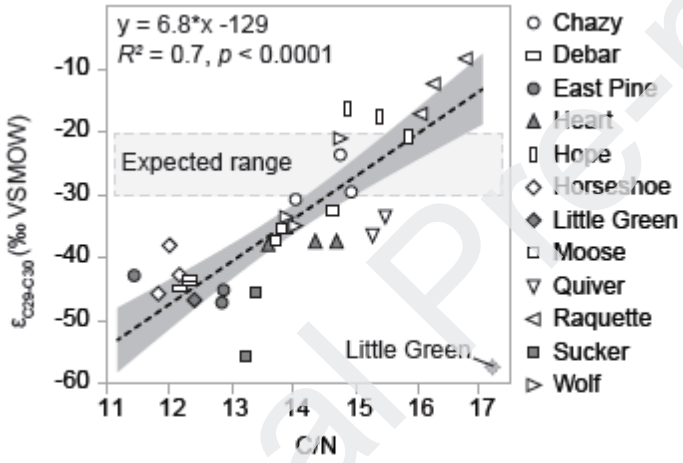

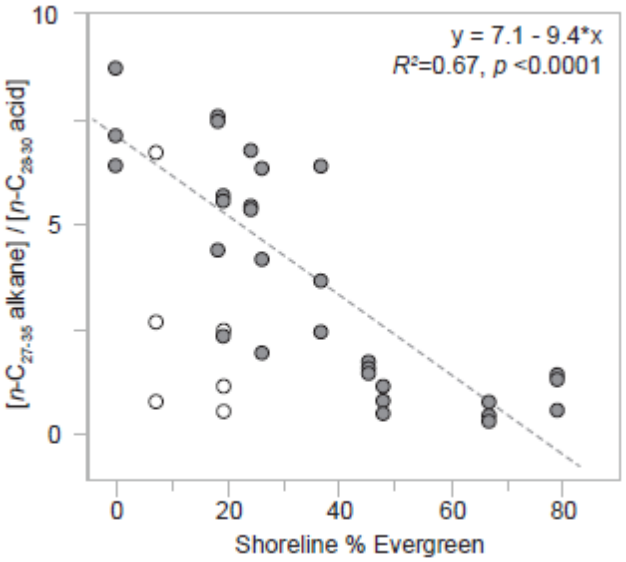

Site	Latitude	Longitude	Elevation (m)	MAT (ºC)	MAP (mm)	Lake area (km^2)	Catchment area (km^2)	Lake/catchment area ratio	Fluvial inlets	Water depth at core site (m)	δ^2H_{MAP} (‰)	Lake water δ^2H (‰)	$\varepsilon_{lw\text{-}MAP}$ $\delta^{18}O$ (‰)	$\delta^{13}C_{org}$ (‰)	TOC (Wt%)	C/N (atomic)
Chazy	44.73	-73.82	466	6.2	1062	7.5	58	0.13	≥1	3.1	-76	-72.8	0.4	-26.8	10.0	14.6
Debar	44.62	-74.19	483	5.3	1138	0.4	6.4	0.06	≥1	9.2	-76	-66.1	1.9	-31.1	18.9	12.3
East Pine	44.34	-74.41	513	5.2	1112	0.3	1.1	0.24	0	10.2	-75	-62.7	2.7	-31.3	29.7	12.4
Heart	44.18	-73.97	665	5.0	1131	0.1	0.8	0.14	0	13.1	-75	-62.5	2.8	-28.5	18.9	14.2
Hope	44.51	-74.13	523	5.2	1127	0.1	0.4	0.28	≥1	9.9	-76	-59.3	3.5	-29.6	29.3	15.4
Horseshoe	44.14	-74.62	524	5.1	1100	1.6	11.5	0.14	≥1	4.0	-74	-59.0	3	-30.5	15.5	12.0
Little Green	44.36	-74.30	521	5.2	1104	0.3	1.4	0.21	0	14.1	-75	-60.2	3.3	-29.3	23.6	14.2
Moose	44.37	-74.06	475	5.2	1052	0.7	17.4	0.04	≥1	20.0	-74	-72.6	0.4	-28.6	17.7	14.1
Quiver	43.74	-74.87	539	5.2	1207	0.1	0.6	0.13	≥1	4.0	-72	-55.5	3.8	-32.0	35.2	15.6
Raquette	44.23	-74.47	470	5.3	1113	4.1	17.1	0.24	≥1	3.8	-74	-70.6	0.5	-28.7	15.4	16.4
Sucker	44.18	-75.12	426	5.8	1134	0.4	2.6	0.14	0	1.8	-74	-45.9	5.4	-28.1	25.2	13.5
Wolf	44.02	-74.22	558	4.9	1121	0.6	4.7	0.13	≥1	13.0	-73	n.d.	n.d.	-28.8	17.7	14.2

Table 1. Location, climate and morphologic data for the 12 sampled lakes. Mean annual temperature (MAT) and mean annual precipitation (MAP) are the 30-year normal (1981-2010) for each location from PRISM. Lake water isotope values are the mean of all samples collected. Bulk surface sediment characteristics represent the mean of three depths (1,5 and 9 cm) from each lake (see table EA-1 for data from all 36 samples). Basins with one or more fluvial inlets are labeled as open. $\varepsilon_{lw\text{-}MAP,}$ fractionation between lake water $\delta^{18}O$ and $\delta^{18}O_{MAP}$.

Table 2. Summary data for common Adirondack plants sampled in May 2017, including xylem water and leaf wax molecular and δ^2H_{wax} composition. Species-level data are summarized by plant type for evergreen gymnosperms (EG) and deciduous angiosperms (DA), pooled by species. $\varepsilon_{C29\text{-}MAP}$ values are based on OIPC-modeled mean annual precipitation at each site; $\varepsilon_{C29\text{-}xw}$ values are based on xylem water from the same individual plant.

Site	Species	Common name	Plant type	Xylem water		ACL		[*n*-$C_{27\text{-}35}$ alkane]/ [*n*-$C_{28\text{-}30}$ acid]	CPI		δ^2H *n*-alkane (‰)			ε_{app} (‰)	
				$\delta^{18}O$	δ^2H	*n*-$C_{27\text{-}35}$ alkane	*n*-$C_{26\text{-}30}$ acid		*n*-$C_{23\text{-}35}$ alkane	*n*-$C_{22\text{-}30}$ acid	*n*-C_{27}	*n*-C_{29}	*n*-C_{31}	$\varepsilon_{C29\text{-}MAP}$	$\varepsilon_{C29\text{-}xw}$
East Pine	*Abies balsamea*	Basalm Fir	EG	-9.6	-74.8	28.4	28.3	0.1	1.3	3.0	-152	-178	-176	-112	-112
East Pine	*Acer rubrum*	Red Maple	DA			30.1	26.6	33.4	15.0	4.8	-162	-191	-194	-125	
East Pine	*Betula papyrifera*	Paper Birch	DA	-9.4	-70.4	27.5	26.4	8.1	4.9	7.1	-166	-161	-160	-93	-98
East Pine	*Pinus strobus*	Eastern White Pine	EG	-10.5	-75.5	28.9	28.0	0.2	1.8		-155	-176	-191	-109	-109
Heart	*Acer rubrum*	Red Maple	DA	-9.4	-64.5	29.9	26.3	51.5	15.1	4.1	-148	-181	-170	-115	-125
Heart	*Betula papyrifera*	Paper Birch	DA	-10.7	-80.9	27.5	26.3	25.6	6.6	5.8	-163	-157		-88	-82
Heart	*Pinus resinosa*	Red Pine	EG	-11.5	-82.6	28.7	27.4	0.5	1.9	3.1	-155	-176	-163	-109	-102
Heart	Shrub 1	Shrub 1	DA	-9.3	-74.5	28.6			9.2		-153	-168		-100	-101
Heart	*Thuja occidentalis*	N. White Cedar	EG	-10.0	-67.3	33.9	26.9	12.5	17.6	4.4					
Heart	*Tsuga canadensis*	Eastern Hemlock	EG	-10.7	-73.5	27.8	27.7	0.1	1.4	3.0	-148	-171	-164	-103	-105
Hope	*Tsuga canadensis*	Eastern Hemlock	EG	-9.7	-71.5	27.8	27.6	0.1	1.4	2.5	-148	-167	-163	-99	-103
Horsesh oe	*Betula papyrifera*	Paper Birch	DA	-11.6	-87.6	27.4	26.9	48.5	12.9	4.3	-170	-168		-102	-89
Little Green	*Acer rubrum*	Red Maple	DA			29.9	26.6	54.2	18.5	4.0	-182	-210	-207	-146	
Little Green	*Betula papyrifera*	Paper Birch	DA	-9.1	-74.5	27.5	26.3	16.5	7.5	7.1	-173	-175	-159	-108	-108
Little	*Fagus*	America	DA	-9.9	-	28.7	26.	3.9	4.7	5.4	-	-		-	-

Green	*grandifolia*	n Beech			68.8		9				157	183		117	123
Little Green	*Picea rubens*	Red Spruce	EG	-10.8	-72.3	28.8	28.6	0.3	1.7	2.4	-146	-185	-170	-119	-121
Little Green	*Pinus strobus*	Eastern White Pine	EG	-8.6	-69.6	28.6	27.5	0.2	1.7		-149	-197	-204	-132	-137
Little Green	*Tsuga canadensis*	Eastern Hemlock	EG	-9.5	-70.8	29.0	27.8	0.3	2.2	3.4	-147	-164	-162	-96	-100
Moose	*Acer rubrum*	Red Maple	DA	-9.3	-76.6	30.3	26.8	68.4	32.0	3.2		-203	-195	-140	-137
Moose	*Betula papyrifera*	Paper Birch	DA	-11.3	-87.0	28.1	26.3	13.4	11.2	4.3	-171	-164	-169	-97	-84
Moose	*Fagus grandifolia*	American Beech	DA	-10.3	-81.0	28.1	27.1	0.9	3.6	3.8	-153	-161		-94	-87
Moose	Shrub 2	Shrub 2	DA	-10.0	-74.5	30.6	27.1	57.9	7.9	5.7	-136	-159	-167	-92	-91
Moose	*Thuja occidentalis*	N. White Cedar	EG	-9.8	-75.2	34.5	26.6	19.1	9.4	3.8					
Moose	*Tsuga canadensis*	Eastern Hemlock	EG	-10.5	-79.6	30.0	27.8	0.5	2.2	3.4	-155	-166	-150	-99	-94
Raquette	*Pinus sylvestris*	Scots Pine	EG	-9.4	-71.8	28.4	27.2	1.5	2.1	2.7	-147	-176		-110	-112
		Mean DA	-10.0	-76.4	28.8	26.6	31.8	10.0	5.0	-161	-175	-178	-109	-102	
		Mean EG	-10.0	-73.7	29.9	27.6	3.9	3.2	3.0	-150	-176	-171	-109	-109	

Site	ACL		[*n*-C_{27-35} alkane]/[*n*-C_{28-30} acid]	CPI		δ^2H *n*-alkane (‰)			δ^2H *n*-acid (‰)		$\varepsilon_{alkane-acid}$ (‰)		ε_{app} (‰)	
	n-C_{27-35} alkane	*n*-C_{26-30} acid		*n*-C_{23-35} alkane	*n*-C_{22-30} acid	*n*-C_{27}	*n*-C_{29}	*n*-C_{31}	*n*-C_{28}	*n*-C_{30}	$\varepsilon_{C29-C30}$	$\varepsilon_{C27-C28}$	$\varepsilon_{C29-MAP}$	$\varepsilon_{C28-MAP}$
Chazy	29.7	26.5	1.4	2.5	2.7	-188	-188	-179	-174	-165	-28	-17	-121	-106
Debar	29.3	26.5	5.8	2.7	2.5	-195	-196	-179	-167	-159	-44	-33	-130	-99
East Pine	29.4	26.4	0.5	4.4	3.7	-199	-193	-180	-158	-155	-45	-48	-128	-90
Heart	29.6	26.6	7.4	2.0	2.9	-187	-186	-174	-155	-154	-38	-39	-119	-86
Hope	29.3	26.5	1.1	3.6	3.3	-202	-190	-176	-171	-175	-18	-37	-123	-103
Horseshoe	29.1	26.5	4.1	2.1	2.6	-187	-188	-176	-167	-152	-42	-25	-123	-100
Little Green	29.6	26.4	0.8	2.4	3.6	-189	-190	-179	-152	-146	-52	-45	-124	-83
Moose	29.7	26.5	1.6	2.4	2.2	-194	-190	-176	-162	-161	-35	-38	-126	-95
Quiver	29.7	26.5	4.1	2.1	4.2	-181	-179	-176	-153	-149	-35	-33	-115	-87
Raquette	29.7	26.6	3.4	2.0	2.4	-189	-186	-167	-180	-176	-13	-12	-121	-114
Sucker	29.4	26.6	4.5	2.7	3.1	-200	-197	-181	-167	-159	-46	-39	-133	-100
Wolf	29.9	26.5	6.5	2.0	2.9	-184	-179	-168	-156	-154	-30	-33	-114	-90
Sediment	29.5	26.5	3.4	2.6	3.0	-191	-188	-176	-164	-159	-35	-33	-123	-97
Plant	29.4	27.1	16.8	6.1	3.8	-156	-175	-174					-109	
Mean DA	28.8	26.6	31.8	10.0	5.0	-161	-175	-178					-109	
Mean EG	29.9	27.6	3.9	3.2	3.0	-150	-176	-171					-109	

Table 3. Mean molecular and δ^2H_{wax} plant wax data from lake surface sediments (n = 36 samples; 3 samples per lake, at 1, 5 and 9 cm depth), for long-chain *n*-alkanes and *n*-alkanoic acids. ε_{app} values are based on OIPC-modeled mean annual precipitation ($\varepsilon_{wax/MAP}$) at each site. Mean values for modern plants (n = 27 individuals) are pooled by total species (n = 12), DA species (n = 5) and EG species (n = 7).